

Dorsal Raphe Dopamine Neurons Modulate Arousal and Promote Wakefulness by Salient Stimuli

Highlights

- DRN^{DA} neurons are activated by salient stimuli irrespective of hedonic valence
- DRN^{DA} activity fluctuates across sleep-wake states and is highest at wakefulness
- Optogenetic activation promotes wakefulness
- Chemogenetic inhibition opposes wakefulness, even in the presence of salient stimuli

Authors

Jounhong Ryan Cho,
Jennifer B. Treweek,
J. Elliott Robinson, Cheng Xiao,
Lindsay R. Bremner, Alon Greenbaum,
Viviana Gradinaru

Correspondence

viviana@caltech.edu

In Brief

Cho et al. demonstrate that dorsal raphe nucleus dopaminergic (DRN^{DA}) activity escalates in response to salient stimuli irrespective of valence, correlates with sleep-wake states, and can bidirectionally modulate arousal.

Dorsal Raphe Dopamine Neurons Modulate Arousal and Promote Wakefulness by Salient Stimuli

Jounhong Ryan Cho,¹ Jennifer B. Treweek,² J. Elliott Robinson,² Cheng Xiao,² Lindsay R. Bremner,² Alon Greenbaum,² and Viviana Gradinaru^{2,3,*}

¹Computation and Neural Systems

²Division of Biology and Biological Engineering

California Institute of Technology, Pasadena, CA 91125, USA

³Lead Contact

*Correspondence: viviana@caltech.edu

<http://dx.doi.org/10.1016/j.neuron.2017.05.020>

SUMMARY

Ventral midbrain dopamine (DA) is unambiguously involved in motivation and behavioral arousal, yet the contributions of other DA populations to these processes are poorly understood. Here, we demonstrate that the dorsal raphe nucleus DA neurons are critical modulators of behavioral arousal and sleep-wake patterning. Using simultaneous fiber photometry and polysomnography, we observed time-delimited dorsal raphe nucleus dopaminergic (DRN^{DA}) activity upon exposure to arousal-evoking salient cues, irrespective of their hedonic valence. We also observed broader fluctuations of DRN^{DA} activity across sleep-wake cycles with highest activity during wakefulness. Both endogenous DRN^{DA} activity and optogenetically driven DRN^{DA} activity were associated with waking from sleep, with DA signal strength predictive of wake duration. Conversely, chemogenetic inhibition opposed wakefulness and promoted NREM sleep, even in the face of salient stimuli. Therefore, the DRN^{DA} population is a critical contributor to wake-promoting pathways and is capable of modulating sleep-wake states according to the outside environment, wherein the perception of salient stimuli prompts vigilance and arousal.

INTRODUCTION

In mammals, behavioral arousal fluctuates as inputs are received from both the external environment (e.g., food availability, predator threat) and internal milieu (e.g., hunger, mating drive, homeostatic sleep demand) (Garey et al., 2003; Brown et al., 2012). While the neural circuits that encode these individual stimuli can be highly stimulus specific or tuned to a specific valence (positive or negative), their activation often promotes more general effects on arousal and electrocortical wakefulness through diverse wake-promoting neurons (Aston-Jones and Bloom, 1981; Szymusiak and McGinty, 2008). Akin to how the noradrenergic (NA) neurons of the locus coeruleus (LC) regulate circadian

sleep-wake cycling (Takahashi et al., 2010) and promote vigilance during wake (Aston-Jones and Bloom, 1981), multiple neural circuits play roles in electrocortical wakefulness and behavioral arousal to motivationally relevant situations, including cholinergic neurons of the pons and basal forebrain (Jones, 1991; Xu et al., 2015; Pinto et al., 2013), the corticotrophin-releasing hormone (CRH) and hypocretin (orexin) neuropeptide systems (Sakurai et al., 1998; Winsky-Sommerer et al., 2005), and the mesolimbic dopamine (DA) system (Eban-Rothschild et al., 2016; Taylor et al., 2016).

Several lines of basic research and clinical observations converge upon DA as a crucial modulator of wake drive, but the neuroanatomical underpinnings have resisted detailed characterization. For example, persistent elevation of DA tone via pharmacology (i.e., amphetamine [Daberkow et al., 2013], modafinil [Qu et al., 2008]) or genetic ablation of the dopamine transporter gene (*Slc6a3*) (Wisor et al., 2001) is associated with behavioral arousal, but these manipulations are diffuse and brain-wide rather than localized to a certain region. Recent work has revealed a role for ventral tegmental area (VTA) DA neurons in electrocortical arousal and sleep-wake patterning (Eban-Rothschild et al., 2016; Taylor et al., 2016), which complements its long-standing role in behavioral arousal to motivationally relevant stimuli (Cohen et al., 2012; Lammel et al., 2014; Matsumoto and Hikosaka, 2009). In contrast, diminished DA signaling from the substantia nigra pars compacta (SNc) is associated with insomnia, a major symptom in Parkinson's disease (Gjerstad et al., 2007). Considering the functional (Morales and Margolis, 2017), genetic (Poulin et al., 2014), and anatomical (Lammel et al., 2011, 2012; Margolis et al., 2008) heterogeneity of midbrain DA neurons, distinct DA subgroups may exert diverging effects on sleep-wake regulation.

Previously, a small population of DA neurons (~1,000 cells in rats) in the dorsal raphe nucleus (DRN; or "A10 dc" or "ventral/ventrolateral periaqueductal gray"; herein referred to as the DRN^{DA}) (Hokfelt et al., 1984; Descarries et al., 1986; Dougalis et al., 2012) was observed to be wake promoting (Lu et al., 2006). Chemical lesion of these cells precipitated profound hypersomnia (~20% increase in sleep), while prolonged wakefulness elicited increased *c-fos* expression (Lu et al., 2006; but see Léger et al., 2010). Compared to other DA populations, little is known about the natural dynamics of DRN^{DA} cells, such as whether their activity contributes to the valuation of external

cues and whether this valuation is predictive of the corresponding behavioral response. Contrary to VTA^{DA}-driven reward circuits, optogenetic activation of DRN^{DA} neurons fails to reinforce operant responding (McDevitt et al., 2014) but instead conveys a negative affective state and promotes social seeking via a negative reinforcement mechanism (Matthews et al., 2016). Given these seemingly disparate roles of DRN^{DA} cells, namely to promote wakefulness (Lu et al., 2006) and encode a “loneliness-like” state (Matthews et al., 2016), we hypothesized that DRN^{DA} neurons may signal arousal on a more general level, including awakening from sleep, maintenance of wakefulness, and promoting arousal in response to behaviorally relevant cues.

Here, we performed longitudinal monitoring of DRN^{DA} activity by calcium imaging via fiber photometry (Gunaydin et al., 2014) and of sleep-wake states via electroencephalography (EEG) and electromyography (EMG) recordings, in conjunction with optogenetics and chemogenetics for reversible, spatially specific control of neural activity (Rajasethupathy et al., 2016; Urban and Roth, 2015). We found that DRN^{DA} neurons are wake-active, showing higher population activity during wakefulness over sleep states, and that endogenous DRN^{DA} activity correlates with state transitions and with external stimulus-driven behaviors. Furthermore, reversible and bi-directional manipulations of DRN^{DA} firing support the sufficiency and necessity of these neurons in promoting vigilance and arousal. Taken together, our results provide evidence that DRN^{DA} pathways provide a circuit for modulating behavioral states and salience-induced arousal in mammals.

RESULTS

DRN^{DA} Neurons Are Activated by Arousal-Provoking Salient Cues

To investigate the natural dynamics of DRN^{DA} neurons during awake-behaving states, we monitored DRN^{DA} population activity in subjects exposed to a diverse array of salient stimuli and environmental settings. In vivo activity of DRN^{DA} neurons was recorded using fiber photometry (Gunaydin et al., 2014), which can measure bulk Ca²⁺-dependent fluorescence of GCaMP6, a genetically encoded calcium indicator (Chen et al., 2013), through a single optical fiber positioned in deep brain structures (Figures S1A, S1G, and S1H). Our photometry setup utilized a 490 nm beam to activate Ca²⁺-dependent GCaMP6 fluorescence, as well as a 405 nm beam to image an isosbestic reference signal, which compensates for photo-bleaching and movement-related artifacts (Lerner et al., 2015). For specific targeting of DRN^{DA} neurons, we stereotactically injected an adenovirus-associated virus (AAV) encoding GCaMP6f in a Cre-dependent manner (AAV5-Syn-FLEX-GCaMP6f) into the DRN of tyrosine hydroxylase (TH)::IRES-Cre mice (Figures 1A and 1B). Control animals were injected with AAV encoding the fluorescent marker EGFP (AAV5-hSyn-DIO-EGFP). An optical fiber was implanted over the DRN to acquire population fluorescence emitted from DRN^{DA} neurons (Figures 1A and S1A). We confirmed that GCaMP6f-expressing neurons emitted dynamic fluorescence fluctuations, while EGFP-expressing cells showed minimal fluorescence variation (Figures S1B and S1C).

We quantified the efficiency and specificity of GCaMP6f+ neurons in the DRN of TH-Cre mice. Transfection was highly efficient (94.2%, n = 407/432 neurons). Similar to previous reports that used the identical mouse line or others targeting TH or the *S/c6a3* promoter (Matthews et al., 2016), 74.9% (n = 407/543) of GCaMP6f+ neurons were co-localized with TH in the DRN. These neurons are not noradrenergic, as they lack dopamine beta-hydroxylase, which converts dopamine to norepinephrine (Nagatsu et al., 1979). Importantly, GCaMP6f+ or TH+ neurons never overlapped with serotonergic neurons (Figures 1B and S1D; Lu et al., 2006; Matthews et al., 2016), a major population in the DRN that is hypothesized to regulate arousal states (Jouvet, 1999). It is possible that GCaMP6f+/TH- neurons may express TH at a level below immunohistochemical detection limit but sufficient to drive Cre expression.

We first tested DRN^{DA}-GCaMP6f mice in a social interaction paradigm, in which physical contact with conspecifics after social isolation has been demonstrated to activate DRN^{DA} neurons (Matthews et al., 2016). We observed the robust activation of DRN^{DA} neurons in single-housed male DRN^{DA}-GCaMP6f mice when they first interacted with female intruders (Figures 1C and 1D). Similar activation was observed with juvenile mice (Figure S2A; Movie S1; Matthews et al., 2016) and also when they displayed aggressive behavior toward adult male intruders (Figure S2B). Beyond social interaction, we also observed prominent DRN^{DA} activity when mice consumed palatable food (Figures 1E and 1F; Movie S2). To further characterize the valence tuning of DRN^{DA} cells, we also challenged DRN^{DA}-GCaMP6f mice in assays with negative contexts. Surprisingly, DRN^{DA} neurons showed phasic activation upon delivery of unexpected electric footshocks (Figures 1G and 1H), air puffs (Figure S2C), or motivated responding (mobility/struggling) in tail suspension tests (Figure S2D) and during investigation of predator odor TMT (component of fox urine; Figure S2E). Furthermore, they showed sustained activation when subjects were physically restrained (Figure S2F).

In contrast, DRN^{DA} activity showed minimal change when mice interacted with novel or familiar objects (Figures 1I–1L, first encounters), which are less salient than social targets, food, or aversive cues. Indeed, DRN^{DA} activation during female interaction, chocolate consumption, and footshock was significantly larger than that during object investigation (Figure 1M). Furthermore, the second and third bouts of female interaction and aggressive behavior continued to provoke a significant elevation in DRN^{DA} activity, whereas it remained relatively unchanged from baseline with repeated novel object encounters, suggesting rapid habituation toward physically salient but motivationally neutral cues (Figures S2G–S2I).

These findings did not vary with subject social history, as similar patterns of DRN^{DA} activation were seen in group-housed mice (Figures S2J–S2L). Furthermore, DRN^{DA} neuronal activation was not correlated with locomotion, which argues against the observed DRN^{DA} activity resulting from the motor response alone (Figures S2M–S2O). Taken together, these findings suggest that DRN^{DA} neurons are activated by a broad array of arousal-provoking stimuli, paralleling animals’ heightened environmental awareness that accompanies exposure to such motivationally salient stimuli.

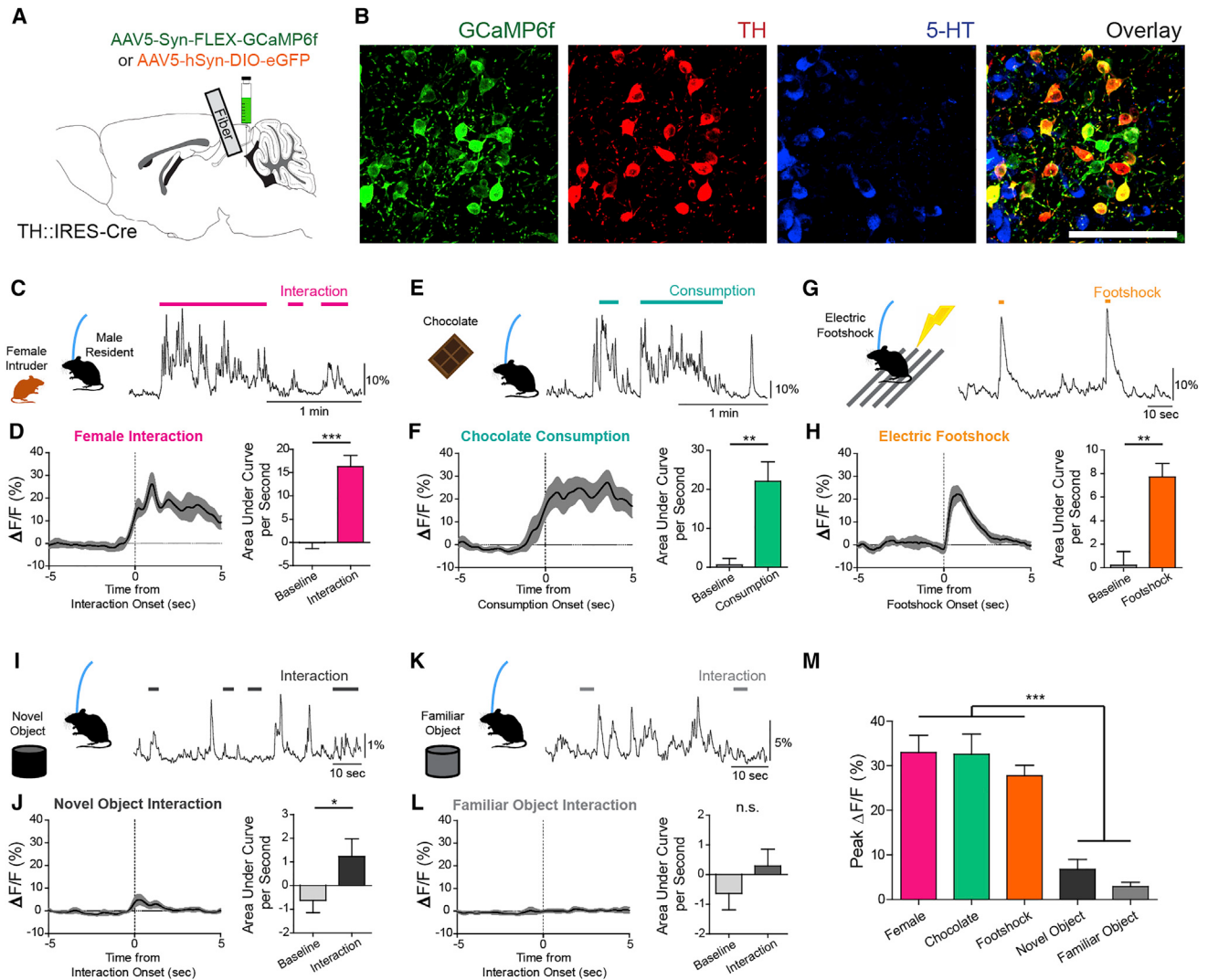


Figure 1. DRN^{DA} Neurons Are Activated upon Exposure to Salient Stimuli or Behavioral Challenge

(A) TH-Cre mice were injected with AAV5-Syn-FLEX-GCaMP6f or AAV5-hSyn-DIO-eGFP and implanted with an optical fiber into the DRN for fiber photometry.

(B) Confocal images of GCaMP6f (green) neurons show co-localization with TH+ neurons (red), but no overlap with 5-HT+ neurons (blue). Scale bar, 100 μ m.

(C) Social interaction between a male DRN^{DA}-GCaMP6f resident mouse and a female intruder were associated with increased DRN^{DA} activity; the trace is a representative recording with interaction bouts indicated.

(D) Left: female interaction caused an increase in fluorescence at the onset (first interactions only). Right: quantification of the area under the curve per second (AUC) during the interaction (0–5 s) shows that social interaction caused significant increase in DRN^{DA} activity from baseline (−5 to 0 s) ($n = 7$ DRN^{DA}-GCaMP6f mice; paired t test, $t_6 = 11.97$, *** $p < 0.001$).

(E) Chocolate consumption by a DRN^{DA}-GCaMP6f mouse increased DRN^{DA} activity; representative recording.

(F) Left: DRN^{DA} activity was increased upon chocolate consumption. Right: AUC quantification during consumption (0–5 s) compared with baseline (−5 to 0 s) shows that food consumption is associated with significant fluorescence increase ($n = 7$ DRN^{DA}-GCaMP6f mice; paired t test, $t_6 = 4.273$, ** $p < 0.01$).

(G) Electric footshocks (0.25 mA, 1 s) were delivered; representative DRN^{DA} trace during two consecutive footshocks.

(H) Left: footshock induced phasic DRN^{DA} activation. Right: DRN^{DA} activity after footshock (0–5 s) was significantly increased relative to baseline (−5 to 0 s) ($n = 7$ DRN^{DA}-GCaMP6f mice; paired t test, $t_6 = 5.763$, ** $p < 0.01$).

(I) DRN^{DA}-GCaMP6f mouse was allowed to interact with a novel object; representative recording during interactions.

(J) Left: first interaction of a novel object was associated with DRN^{DA} activity increase. Right: DRN^{DA} activity after first interaction (0–5 s) was significantly increased relative to baseline (−5 to 0 s) ($n = 7$ DRN^{DA}-GCaMP6f mice; paired t test, $t_6 = 3.614$, * $p < 0.05$).

(K) A familiar object was introduced; representative DRN^{DA} trace with interaction bouts.

(L) Left: first interaction bout was not associated with any change in DRN^{DA} fluorescence. Right: there was no change in DRN^{DA} activity across familiar object interaction ($n = 7$ DRN^{DA}-GCaMP6f mice; paired t test, $t_6 = 2.205$, $p > 0.05$).

(M) Peak DRN^{DA} fluorescence values during female interaction, chocolate consumption, and electric footshocks were significantly higher than those during novel and familiar object interaction ($n = 7$ DRN^{DA}-GCaMP6f mice; one-way ANOVA, $F_{4,30} = 22.77$, $p < 0.0001$, Bonferroni post hoc analysis, *** $p < 0.001$).

Data represent mean \pm SEM.

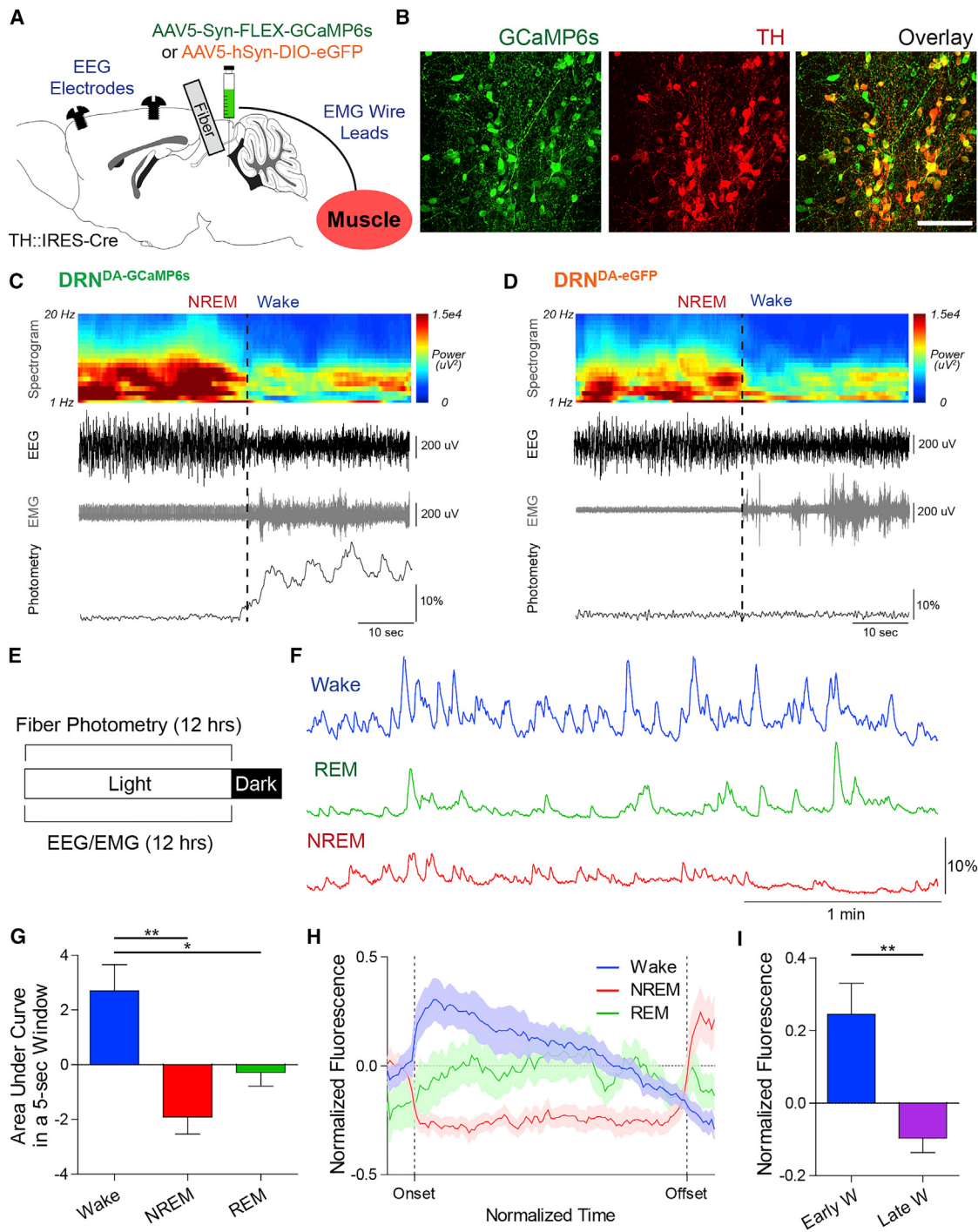


Figure 2. Simultaneous Fiber Photometry and EEG/EMG Recordings Reveal a Correlation between DRN^{DA} Neuronal Activity and Sleep-Wake States

- (A) In addition to fiber photometry, EEG screw electrodes and EMG wires were implanted to classify sleep-wake states.
- (B) Representative confocal images of GCaMP6s+ neurons (green) co-localized with TH+ neurons (red). Scale bar, 100 μm .
- (C) Representative example of an NREM-to-wake transition from a DRN^{DA}-GCaMP6s mouse with EEG spectrogram, EEG, EMG, and photometry traces. Note DRN^{DA} fluorescence was increased at the wake onset, when EEG desynchronized from delta (0.5–4 Hz) and EMG amplitude increased.
- (D) Same as (C), but from a DRN^{DA}-eGFP mouse. No change in photometry was observed.
- (E) Synchronized photometry and EEG/EMG recordings were performed during the entire light phase.
- (F) Representative photometry traces at distinct sleep-wake states (blue, wake; green, REM sleep; red, NREM sleep).

(legend continued on next page)

DRN^{DA} Population Activity Correlates with Sleep-Wake States

That DRN^{DA} neurons were activated by exposure to a variety of salient cues expands their previous description as a socio-centric pathway (Matthews et al., 2016). It seems plausible that DRN^{DA} neurons convey more generalized arousal signals across broad temporal scales, especially given that chemogenetic activation promotes analgesia (Li et al., 2016) and selective lesion causes hypersomnia (Lu et al., 2006).

To test this hypothesis, we prepared TH-Cre mice for simultaneous and synchronized recording of DRN^{DA-GCaMP6s} fluorescence (AAV5-Syn-FLEX-GCaMP6s, EGFP for control animals; DRN optical fiber insertion; Figures 2A and 2B) and polysomnography signals (implantation of EEG electrodes and EMG wires; Figure 2A). Sleep-wake states, which were manually classified in 5 s windows based on the visual and spectral characteristics of the EEG/EMG signals, were correlated to fluctuations in DRN^{DA} population activity (Figures 2C and S3A). Variations in fluorescent signal were absent in control DRN^{DA-EGFP} mice (Figures 2D and S3B), and viral delivery of transgenes (here and in all subsequent experiments) did not alter the basic sleep-wake architecture (Figures S1E and S1F).

To record DRN^{DA} activity over many episodes of distinct sleep-wake states, we collected fiber photometry and EEG/EMG across the entire light (inactive) phase (Figure 2E). DRN^{DA-GCaMP6s} mice showed normal EEG spectral characteristics and sleep-wake patterns, even in the presence of GCaMP6s excitation light (Figures S3C and S3D). Over long recording sessions, GCaMP6s bleaching was observed, but it could be effectively removed by subtracting the linearly scaled control signal from 405 nm excitation (Figure S3E). To examine the correlation of DRN^{DA} activity with sleep-wake states, we calculated the area under the curve (AUC) for non-overlapping 5 s windows of photometry data during each state as an index of the estimated DRN^{DA} population firing rate (Figure 2F). AUC values were significantly higher during wakefulness (Figure 2G). For further characterization, Ca²⁺ peak events were detected (Figure S3F), and their quantitative features were compared across states. The peak amplitude and summed AUC values of detected events were highest during wakefulness, but there was no significant difference in their frequency or duration across distinct states (Figures S3G–S3J). Altogether, these results suggest that DRN^{DA} neurons are wake-active and that their activity profile correlates with arousal states.

To examine the temporal dynamics of DRN^{DA} activity during each state, we normalized the variable durations of sleep-wake states to a unit-less time from 0 (onset) to 1 (offset) and accordingly down-sampled the normalized photometry traces. During wakefulness, DRN^{DA} population fluorescence peaked soon after wake onset and gradually decreased toward wake offset (Figure 2H). Indeed, the DRN^{DA} activity at the early 20th percentile

of a wake episode was significantly larger than at the late 20th percentile (Figure 2I). In contrast, DRN^{DA} activity was continuously suppressed during NREM sleep and showed minimal variations during REM sleep (Figure 2H). We additionally verified that wake episodes whose durations were similar to sleep episodes demonstrated similar dynamics (Figure S3K), suggesting that the observed DRN^{DA} wake dynamics did not originate from photobleaching over time. In sum, the activity level of DRN^{DA} populations not only varies across sleep-wake states but also shows dynamic changes within wakefulness, showing highest activity after wake onset and gradual decrease toward sleep onset.

Next, we examined DRN^{DA} activity during state transitions. DRN^{DA} fluorescence increased significantly at NREM to wake (Figure 3A; when wake duration >60 s). There was no significant fluorescence change at REM-to-wake transitions (Figure 3B; when wake duration >60 s). Conversely, DRN^{DA} activity decreased when animals fell asleep (Figure 3C). We also observed a gradual increase of DRN^{DA} activity across NREM-to-REM transitions (Figure 3D). When a brief period of wake (<15 s) intervened in transition from REM to NREM, DRN^{DA} activity exhibited a corresponding decrease across the brief wake and NREM onset (Figure S3L).

Interestingly, we observed that the duration of wake episodes varied as a function of the change in DRN^{DA} activity across the wake onset. The net fluctuation in DRN^{DA} fluorescence across sleep-to-wake transitions (from both NREM and REM) was significantly larger when mice were awake for a longer period (“long”: >60 s) than when mice were briefly awake (“short”: <30 s; “intermediate”: between 30 and 60 s; Figures 3E and 3F). This suggests that DRN^{DA} activity at wake onset is positively correlated with the duration of the following wake episode. In sum, these results provide correlative evidence that endogenous DRN^{DA} firing is highest during wakefulness and that DRN^{DA} activity is dynamic across state transitions.

Optogenetic Activation of DRN^{DA} Neurons Promotes Wakefulness

To reveal a causal relationship between DRN^{DA} activity and wakefulness, we tested for sufficiency using a Cre-dependent excitatory opsin to stimulate transduced DRN^{DA} cells (AAV5-Ef1a-DIO-ChR2-eYFP, EGFP for controls; polysomnography for stage classification; Figures 4A and 4B). ChR2-eYFP expression was limited to the DRN and caudal linear nucleus, and never found in retrorubral field or VTA (Figures S4N and S4O). To avoid potential ceiling effects, we applied optogenetic stimulation to DRN^{DA} neurons during the light phase (Figure 4C). As endogenous firing characteristics of DRN^{DA} cells are unknown (one neuron reported by juxtacellular recording [Schweimer and Ungless, 2010]), we used stimulus parameters commonly adopted for photoactivation of ventral midbrain DA neurons (Tsai et al., 2009), which operate in phasic and tonic firing modes. We

(G) Quantification of AUC per 5 s window revealed higher DRN^{DA} activity during wakefulness over NREM and REM sleep ($n = 6$ DRN^{DA-GCaMP6s} mice; one-way ANOVA, $F_{2,15} = 10.58$, $p < 0.01$; Bonferroni post hoc analysis, * $p < 0.05$, ** $p < 0.01$).

(H) Temporal dynamics of normalized DRN^{DA} activity during wake (blue), NREM (red), and REM (green) episodes within normalized time.

(I) Normalized DRN^{DA} activity at early wake (first 20th percentile) was significantly increased from late wake period (last 20th percentile) ($n = 6$ DRN^{DA-GCaMP6s} mice; paired t test, $t_5 = 5.672$, ** $p < 0.01$).

Data represent mean \pm SEM.

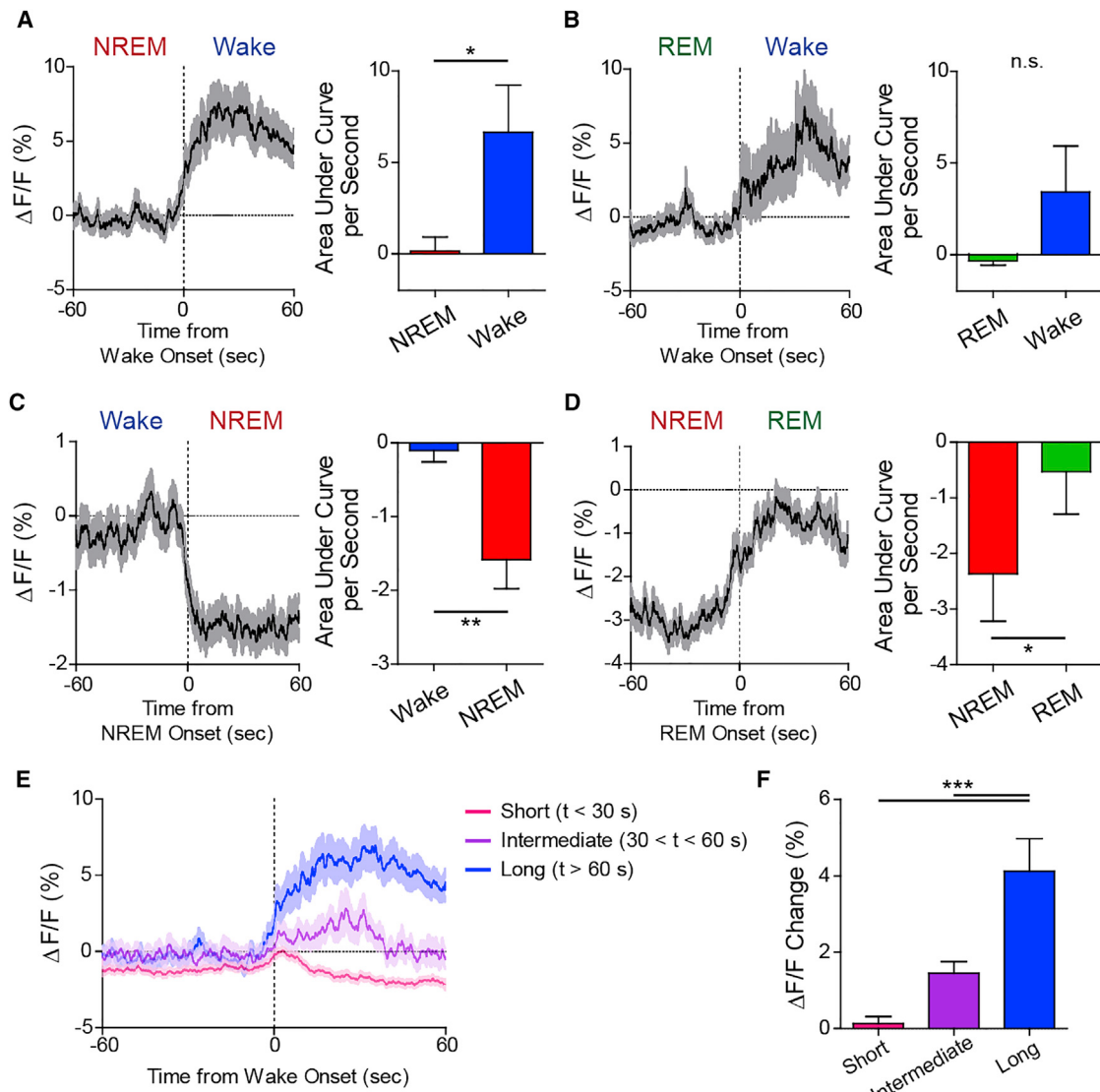


Figure 3. DRN^{DA} Neuronal Dynamics across State Transitions

(A) Left: DRN^{DA} activity increased across NREM-to-wake transitions. Right: DRN^{DA} activity after transitions (wake) was significantly greater than before transitions (NREM) ($n = 6$ DRN^{DA-GCaMP6s} mice; paired t test, $t_5 = 3.052$, $p < 0.05$).

(B) Left: DRN^{DA} activity did not change across REM-to-wake transitions. Right: DRN^{DA} fluorescence was not different across transitions ($n = 6$ DRN^{DA-GCaMP6s} mice; paired t test, $t_5 = 1.556$, $p > 0.1$).

(C) Left: DRN^{DA} activity decreased at wake-to-NREM transitions. Right: the AUC values after transitions (NREM) were significantly lower than before transitions (wake) ($n = 6$ DRN^{DA-GCaMP6s} mice; paired t test, $t_5 = 4.516$, $**p < 0.01$).

(D) Left: DRN^{DA} fluorescence increased across NREM-to-REM transitions. Right: DRN^{DA} activity significantly increased during NREM to REM transitions ($n = 6$ DRN^{DA-GCaMP6s} mice; paired t test, $t_5 = 3.192$, $*p < 0.05$).

(E) DRN^{DA} activity increase across sleep-to-wake transitions was more prominent when mice spent longer time awake (> 60 s, blue) than when mice were awake for intermediate (between 30 and 60 s, purple) or short (< 30 s, pink) period.

(F) Fluorescence increase across wake onsets was significantly larger for long-duration wake episodes than for intermediate- or short-duration wake episodes ($n = 366$ short, 158 intermediate, and 185 long wake episodes; one-way ANOVA, $F_{2,706} = 21.85$, $p < 0.0001$; Bonferroni post hoc analysis, *** $p < 0.001$). Data represent mean \pm SEM.

applied both phasic (a train of ten 30 Hz pulses, 10 ms pulse width, every 5 s) and tonic (continuous 2 Hz pulses, 10 ms pulse width) stimulation patterns (Figures 4C and S4D). These specific parameters were designed to expose subjects to the same total number of light pulses with distinct temporal structures. We veri-

fied that DRN^{DA} neurons were capable of faithfully following phasic pulse trains in whole-cell patch clamp recordings (Figure S4A).

Two minutes of phasic stimulation caused immediate transitions to and maintenance of wakefulness from both NREM and

REM sleep in DRN^{DA-ChR2} mice, but not in control DRN^{DA-EGFP} mice (Figures 4D–4F, S4B, and S4C). By contrast, 2 min of tonic stimulation could only induce waking from REM sleep (Figures S4D–S4G). Because phasic stimulation more reliably evoked stage changes, we employed this paradigm in subsequent experiments. Phasic activation was effective in inducing immediate NREM-to-wake transitions even after 4 hr of sleep deprivation, suggesting that DRN^{DA} activation can promote instantaneous arousal in face of high sleep pressure (Figure 4G). Phasic stimulation caused a significant change in cortical EEG in DRN^{DA-ChR2}, but not in control DRN^{DA-EGFP} mice, as revealed by spectral analysis (Figures 4H, 4I, S4H, and S4I); delta (0.5–4 Hz) and high-frequency (40–100 Hz) EEG powers were decreased and increased, respectively, upon DRN^{DA} activation (Figures 4J and 4K).

We next sought to examine the effect of longer, sustained activation of DRN^{DA} neurons on behavioral states. A 1 hr epoch of phasic stimulation was applied 4 hr into the subject's light phase when sleep pressure is high. Photostimulation resulted in a net increase in time awake relative to unstimulated epochs, due to the extension of wake episodes (Figures 4L and 4M). Spectral analysis revealed that delta (0.5–4 Hz) power was significantly diminished while high-frequency (40–100 Hz) activity was enhanced in ChR2-expressing mice (Figures 4N–4P). This spectral change from DRN^{DA} activation could not be attributed to increased locomotion, which can also affect cortical activity and arousal (Vinck et al., 2015), because optogenetic manipulations did not affect locomotion in either the light or dark phase (open field test; Figure S4L). Moreover, the sustained increase in wakefulness from DRN^{DA} activation was directly mediated by DA, as systemic administration of D1 and D2 receptor antagonists (SCH-23390 and eticlopride, respectively, 1 mg/kg) prior to stimulation abolished the wake-promoting effect of phasic stimulation in DRN^{DA-ChR2} mice but caused no overall effect in control mice (Figures S4J–S4K).

In sum, phasic stimulation of DRN^{DA} neurons can affect sleep-wake state patterning and promote arousal by inducing immediate sleep-to-wake transitions and prolonging wake duration. DRN^{DA} activity also causes electrocortical arousal, bi-directionally modulating low- and high-frequency rhythms across both minutes-short and hour-long temporal scales.

Chemogenetic Inhibition of DRN^{DA} Neurons Reduces Wakefulness

To interrogate the necessity of DRN^{DA} signaling for wake maintenance, we used a chemogenetic (Urban and Roth, 2015) approach to reversibly inhibit DRN^{DA} activity during polysomnographic recordings (Figure 5A). Here, DRN^{DA} cell recruitment via expression of the inhibitory DREADD (AAV2-hSyn-DIO-hM4Di-mCherry; Figures 5A and 5B) rather than the analogous opsin is not limited to light spread from optical fibers, and long-term suppression of DRN^{DA} activity carries no potential for phototoxicity. We confirmed with ex vivo whole-cell patch-clamp recordings that bath application of 1 μM clozapine-N-oxide (CNO) reversibly reduced the firing of hM4Di-expressing DRN^{DA} neurons via hyperpolarization but showed no effect on EGFP-positive cells in control mice (Figures S5B–S5E). We also verified that the hM4Di vector was not anterogradely or retrogradely

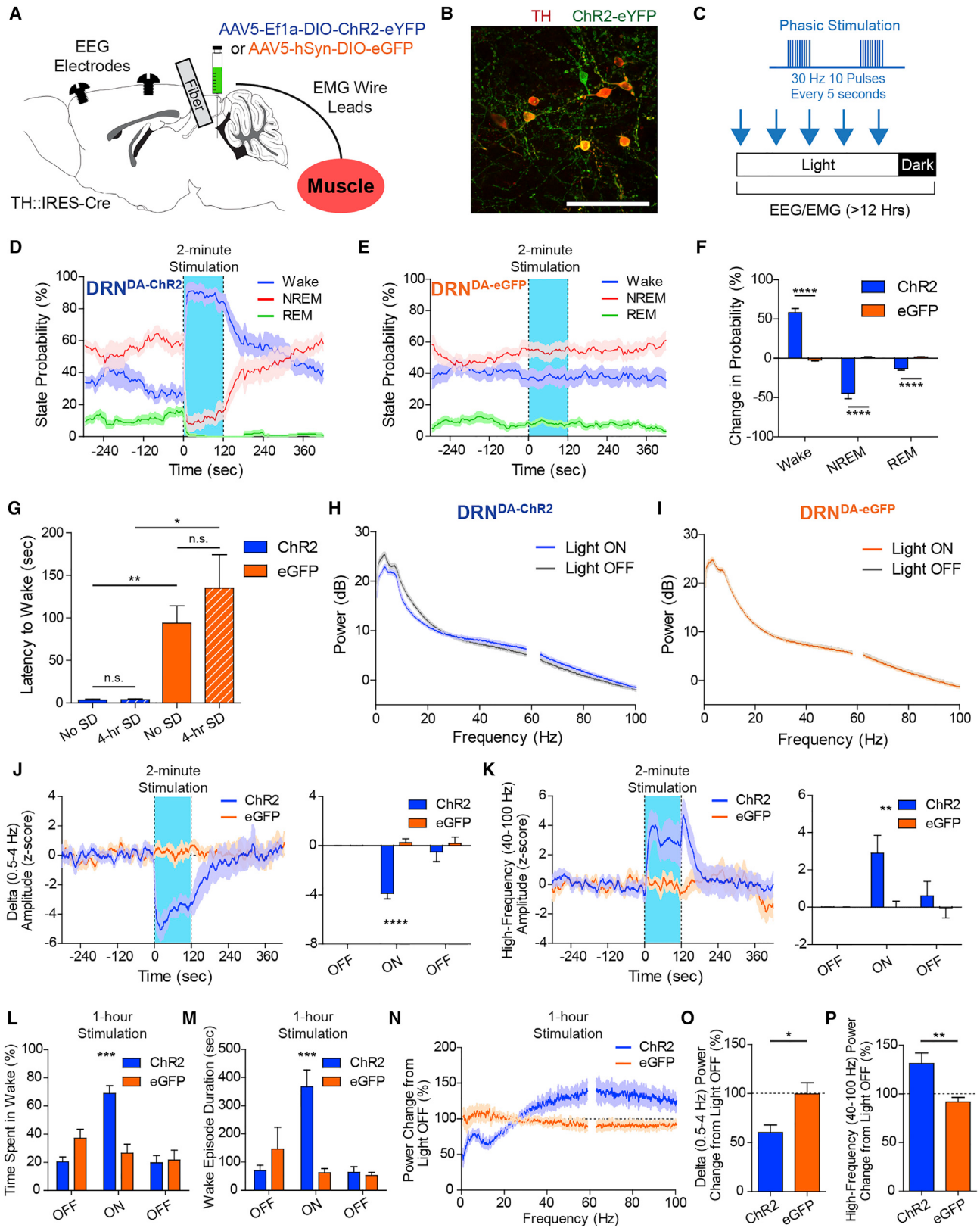
transported from the DRN to other TH+ neurons (across a 4-week window; Figures S5F–S5I), some of which have been shown to have reciprocal connections (Lu et al., 2006).

DRN^{DA-hM4Di} and DRN^{DA-EGFP} mice were habituated to experimenter handling for three days prior to intraperitoneal injection of saline or CNO (1 mg/kg) 3 hr into their dark (active) cycle, and EEG/EMG recordings took place for 2 hr afterward (Figure 5C). Compared to saline, CNO injection led to a marked reduction in wakefulness (Figures 5D and 5E). At the group level, DRN^{DA} inhibition decreased the time spent in wakefulness and increased NREM sleep time (Figure 5F). Specifically, CNO injection into the DRN^{DA-hM4Di} mice increased NREM sleep duration (Figure 5G) but had no effect on the number of episodes of each state (Figure 5H). Importantly, saline or CNO injection into control mice did not affect sleep-wake proportions (Figures 5F–5H). A change was also evident in cortical EEG (Figure 5I); contrary to optogenetic activation, chemogenetic inhibition was associated with increased delta (0.5–4 Hz) power (Figure 5J) and decreased high-frequency (40–100 Hz) activity (Figure 5K) relative to vehicle injection. To test whether CNO-induced sleep-wake states have normal EEG architecture, we verified that the EEG spectrum in each state after CNO injection was not distinguishable from those after saline injection (Figures S5J–S5L). Thus, our findings indicate that DRN^{DA} neuronal activity is required for supporting wakefulness in normal physiological conditions.

DRN^{DA} Neuronal Activity Supports Wakefulness in the Presence of Salient Stimuli

Since diverse salient stimuli activated DRN^{DA} neurons (Figure 1) and their firing promoted wakefulness (Figures 4 and 5), we asked whether DRN^{DA} neurons are necessary for maintaining arousal in the face of environmental salience by chemogenetically inhibiting their activity (Figure 6A). We introduced female mouse and predator odor TMT to the subject's home cage during the dark cycle while monitoring behavioral states. These two stimuli, which were shown to induce robust DRN^{DA} activity (Figures 1C, 1D, and S2E), hold ethological relevance and are of opposite valence. CNO injection into the DRN^{DA-hM4Di} mice reduced the time spent awake and promoted NREM sleep in both assays, contrary to other conditions where mice remained awake (Figures 6B and 6C). More broadly, DRN^{DA} inhibition during these assays caused a shift in cortical EEG spectra; CNO treatment of DRN^{DA-hM4Di} mice led to an increase in delta (0.5–4 Hz) power and decreases in high-theta (8–12 Hz) and high-frequency (40–100 Hz) power relative to saline condition, which was absent in control mice (Figures 6D–6G).

We further asked if the unexpected presentation of arousing or alerting stimuli (e.g., loud noises) during sleep could induce immediate wake transitions with DRN^{DA} firing. DRN^{DA-GCaMP6s} mice were exposed to randomized auditory stimuli (65 dB, 2–5 kHz, 2 Hz pulse frequency, 250 ms width, 10 s duration) throughout their light phase while recording GCaMP6s fluorescence and EEG/EMG signals (Figure S6A). We observed time-locked DRN^{DA} activity upon tone onset, which was most prominent when subjects immediately (within 10 s) switched from sleep to wake (Figures S6B and S6C). There was no detectable difference in DRN^{DA} activity increase between NREM- and REM-to-wake transitions (Figures S6D and S6E). To test



(legend on next page)

for a causal contribution of DRN^{DA} activity to cued arousal, we repeated the above experiment on mice expressing archaerhodopsin-3 (Arch; Mattis et al., 2011), which allows for time-locked reversible inhibition (Figures S6F and S6G). When DRN^{DA} neurons were exposed to a continuous 20 s light pulse (532 nm, 10 mW) centered on tone delivery (70 dB), the probability of cued waking from NREM (Figures S6H–S6K), but not from REM sleep (Figures S6L–S6O), significantly decreased. DRN^{DA} inhibition did not completely block NREM-to-wake transitions, which suggests that multiple pathways likely work together to sustain full arousal, including, but not limited to, noradrenergic or cholinergic neurons (Aston-Jones and Bloom, 1981; Xu et al., 2015). In sum, these data indicate that DRN^{DA} activity is required for maintaining salience-induced wakefulness and for triggering cued waking from sleep.

DISCUSSION

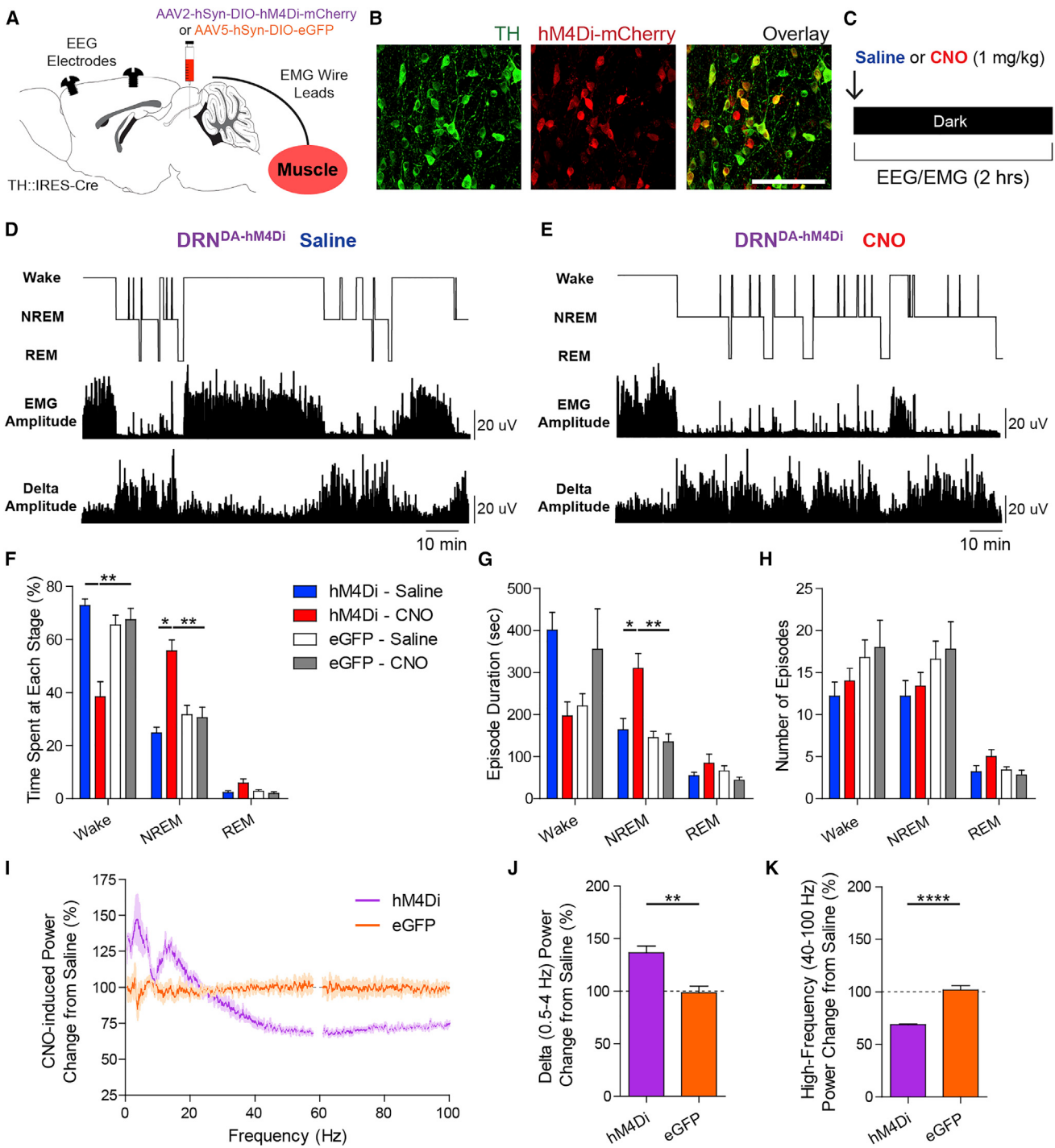
Using simultaneous calcium imaging and polysomnography in conjunction with optogenetic and chemogenetic manipulations, we demonstrated that DRN^{DA} neurons respond to external salient events of positive and negative valence, show correlative fluctuations at the population level across distinct sleep-wake states, and promote wakefulness. Furthermore, DRN^{DA} activity is necessary to maintain normal levels of wakefulness and support arousal in response to the perception of salient stimuli. These findings support a role for wake-promoting DRN^{DA} neurons that parallels the arousal-promoting function of isolated DA cells in invertebrates (Pimentel et al., 2016), as well as a

more expansive role for DRN^{DA} signaling beyond promoting social interaction via negative reinforcement (Matthews et al., 2016) or mediating anti-nociceptive effects (Li et al., 2016).

Our photometry data demonstrate not only that social interaction robustly enhances DRN^{DA} spiking (female interaction, male intruder; Figures 1 and S2), akin to previous findings (juvenile interaction; Matthews et al., 2016), but also that these neurons respond to the perception of highly salient, non-social stimuli (Figures 1 and S2). DRN^{DA} activation by a wide variety of rewarding and aversive stimuli, both social and non-social, occurred irrespective of the subject's social history, as the stimulus-evoked change in DRN^{DA} fluorescence was not influenced by chronic separation from cage-mates (Figures S2J–S2M). Given the subtleties in how various forms of social deprivation (e.g., maternal separation, acute or chronic social isolation) can differentially alter physiology and behavior (George et al., 2010; Whitaker et al., 2013), the extent to which a subject's social environment and rank causes plasticity in DRN^{DA} neurons will require further investigation. Based on the documented heterogeneity of ventral midbrain DA groups (Bromberg-Martin et al., 2010; Morales and Margolis, 2017), it is plausible that DRN^{DA} cells may also be heterogeneous and individually tuned to specific classes of stimuli. For example, some DRN^{DA} neurons may play a general role in social engagement or may be more susceptible to changes in social history, while other subsets may fire selectively for arousing, non-social stimuli. Since we and Matthews et al. (2016) used different fiber-placement methods (angled versus perpendicular, respectively), we may have sampled distinct, non-overlapping DRN^{DA} subsets.

Figure 4. Optogenetic Stimulation of DRN^{DA} Neurons Promotes Wakefulness

- (A) TH-Cre mice injected with AAV5-Ef1a-DIO-ChR2-eYFP or AAV5-hSyn-DIO-EGFP and implanted with an optical fiber received optogenetic stimulation during sleep-wake state monitoring.
 - (B) Confocal images of ChR2-eYFP+ neurons (green) co-localized with TH+ neurons (red). Scale bar, 100 μm.
 - (C) Two-minute blocks (blue arrows) of phasic stimulations were delivered with intervals of 20 to 25 min throughout the light phase to photo-activate DRN^{DA} neurons.
 - (D) Probability of being awake was dramatically increased upon onset of the phasic stimulation, with concurrent reduction of both NREM and REM state probability in DRN^{DA-ChR2} mice.
 - (E) Same as (D), but no change was observed in DRN^{DA-EGFP} mice.
 - (F) The increase in wake probability in DRN^{DA-ChR2} mice compared with DRN^{DA-EGFP} mice was significant, as were the decreases in NREM and REM sleep probability ($n = 8$ per group; unpaired t test, *** $p < 0.0001$).
 - (G) There was no difference in the latency to wake onset even after 4 hr of sleep deprivation in both groups ($n = 4$ per group; paired t test, $p > 0.2$). Regardless of sleep deprivation, latency to wake after stimulation was significantly shorter in DRN^{DA-ChR2} mice compared to controls (unpaired t test, * $p < 0.05$, ** $p < 0.01$).
 - (H) Power spectral density of frontal EEG shows reduced power in low-frequency range and increased power in high-frequency range during light ON (blue) compared to light OFF (gray) conditions in DRN^{DA-ChR2} mice.
 - (I) Same as (H), but power spectral density showed no difference across light ON (orange) and OFF (gray) conditions in DRN^{DA-EGFP} mice.
 - (J) Left: time-varying spectral analysis showed that the amplitude of delta (0.5–4 Hz) rhythms was decreased upon phasic stimulation. Right: delta amplitude during the light ON epoch was significantly decreased compared to baseline OFF epochs ($n = 8$ per group; two-way ANOVA revealed group × epoch interaction, $F_{2,26} = 17.06$, $p < 0.0001$; Bonferroni post hoc analysis, *** $p < 0.0001$).
 - (K) Left: the amplitude of high-frequency (40–100 Hz) rhythms was increased upon phasic stimulation. Right: high-frequency amplitude was significantly increased during the light ON epoch compared to the OFF epochs ($n = 8$ per group; two-way ANOVA revealed group × epoch interaction, $F_{2,26} = 5.096$, $p < 0.05$; Bonferroni post hoc analysis, ** $p < 0.01$).
 - (L) 1 hr of phasic DRN^{DA} stimulation significantly increased the time spent in wakefulness during the light ON hour compared to the light OFF hours ($n = 6$ per group; two-way ANOVA revealed group × epoch interaction, $F_{2,20} = 15.99$, $p < 0.0001$; Bonferroni post hoc analysis, *** $p < 0.001$).
 - (M) 1 hr of phasic stimulation significantly increased the duration of wake episodes ($n = 6$ per group; two-way ANOVA revealed group × epoch interaction, $F_{2,20} = 12.16$, $p < 0.001$; Bonferroni post hoc analysis, *** $p < 0.001$).
 - (N) Power spectral density revealed decrease in low-frequency power and increase in high-frequency power in DRN^{DA-ChR2} mice during light ON compared to the light OFF hours, but no changes were observed in DRN^{DA-EGFP} mice.
 - (O) Stimulation-induced delta (0.5–4 Hz) power reduction was significantly larger in DRN^{DA-ChR2} mice ($n = 6$ per group; unpaired t test, * $p < 0.05$).
 - (P) Stimulation-induced high-frequency (40–100 Hz) power increase was significantly larger in DRN^{DA-ChR2} mice ($n = 6$ per group; unpaired t test, ** $p < 0.01$).
- Data represent mean ± SEM.

**Figure 5. Chemogenetic Inhibition of DRN^{DA} Neurons Reduces Wakefulness**

(A) AAV2-hSyn-DIO-hM4Di-mCherry or EGFP vectors were injected to the DRN of TH-Cre mice, and EEG/EMG electrodes were implanted for sleep-wake state classification.

(B) Confocal images of TH+ (green) neurons co-localized with hM4Di-mCherry (red) expression. Scale bar, 100 μ m.

(C) Saline or CNO (1 mg/kg) was intraperitoneally injected to inhibit DRN^{DA} neurons during the dark phase. EEG/EMG recordings were performed for 2 hr afterward.

(D) Representative hypnogram (top), EMG amplitude (middle, in 5 s windows), and delta amplitude (bottom, in 5 s windows) from a DRN^{DA}-hM4Di mouse after saline injection.

(E) Same as (D), but with CNO injection. CNO injection caused reduced wakefulness, accompanied by lower EMG and higher delta amplitudes.

(legend continued on next page)

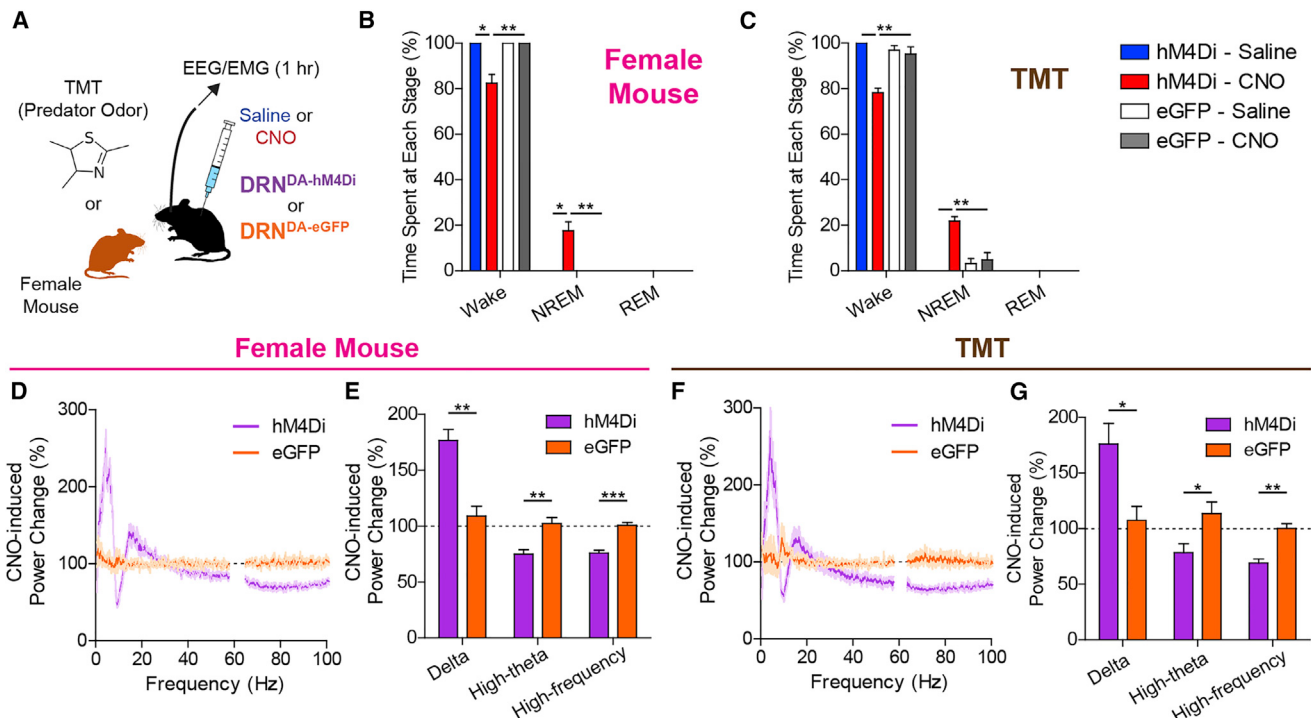


Figure 6. DRN^{DA} Firing Supports Wakefulness upon Exposure to Salient Stimuli

(A) DRN^{DA-hM4Di} and DRN^{DA-eGFP} mice were systemically administered with saline or CNO (1 mg/kg) 45 min prior to the introduction of a female mouse or a filter paper with predator odor TMT. EEG/EMG recordings were carried out for 1 hr after salient stimuli presentation.

(B) While the introduction of a female mouse induced robust wakefulness in other conditions, CNO-injected DRN^{DA-hM4Di} mice spent significantly reduced time in wakefulness at the cost of NREM sleep ($n = 4$ per group; two-way ANOVA revealed a group \times drug interaction, $F_{1,15}$ [wake, NREM] = 20.83, $p < 0.01$, Bonferroni post hoc analysis, * $p < 0.05$, ** $p < 0.01$).

(C) Similar to (B), but a filter paper with predator odor TMT was introduced to home-cages. Compared to other conditions, CNO-injected DRN^{DA-hM4Di} mice spent significantly reduced time in wakefulness and increased time in NREM sleep ($n = 4$ per group; two-way ANOVA revealed a group \times drug interaction, $F_{1,15}$ [wake, NREM] = 26.88, $p < 0.01$, Bonferroni post hoc analysis, ** $p < 0.01$).

(D) Power spectral density analysis during female mouse interaction revealed CNO-induced increase in low-frequency power and decrease in high-theta (8–12 Hz) and high-frequency power in DRN^{DA-hM4Di} mice with respect to the saline condition but no change in control mice.

(E) CNO-induced increase in delta (0.5–4 Hz) power and decrease in high-theta (8–12 Hz) and high-frequency (40–100 Hz) power were significantly larger in DRN^{DA-hM4Di} mice than in controls ($n = 4$ per group; unpaired t test, ** $p < 0.01$, *** $p < 0.001$).

(F) Same as (D), but for the TMT condition. A similar trend was observed as (D).

(G) CNO-induced increase in delta (0.5–4 Hz) power and decrease in high-theta (8–12 Hz) and high-frequency (40–100 Hz) power were significantly larger in DRN^{DA-hM4Di} mice than in controls ($n = 4$ per group; unpaired t test, * $p < 0.05$, ** $p < 0.01$).

Data represent mean \pm SEM.

Matthews et al. (2016) further demonstrated that DRN^{DA} neurons signal aversion, a trend that was also corroborated, albeit weakly, by our data (Figure S4M). This is in stark contrast with

wake-promoting VTA^{DA} neurons, whose activity supports robust place preference and operant responding (Tsai et al., 2009; Witten et al., 2011). That neural circuits may be involved in two

(F) CNO injections into the DRN^{DA-hM4Di} mice decreased the time spent in wake and increased the time spent in NREM sleep ($n = 5$ per group; two-way ANOVA revealed a group \times drug interaction in wake and NREM, $F_{1,19}$ [wake] = 20.96, $p < 0.01$, $F_{1,19}$ [NREM] = 28.34, $p < 0.001$, $F_{1,19}$ [REM] = 2.07, $p > 0.1$; Bonferroni post hoc analysis, * $p < 0.05$, ** $p < 0.01$).

(G) Duration of NREM sleep was significantly increased when DRN^{DA-hM4Di} mice were administered with CNO ($n = 5$ per group; two-way ANOVA revealed a group \times drug interaction in NREM, $F_{1,19}$ [wake] = 3.84, $p > 0.05$, $F_{1,19}$ [NREM] = 10.78, $p < 0.05$, $F_{1,19}$ [REM] = 0.26, $p > 0.6$; Bonferroni post hoc analysis, ** $p < 0.01$, * $p < 0.05$).

(H) There was no difference in the number of episodes in all states ($n = 5$ per group; two-way ANOVA revealed no group \times drug interaction, $F_{1,19}$ [wake] = 0.88, $F_{1,19}$ [NREM] = 0.52, $F_{1,19}$ [REM] = 0.55, all $p > 0.3$).

(I) Power spectral density analysis revealed CNO-induced increase in low-frequency power and decrease in high-frequency power in DRN^{DA-hM4Di} mice with respect to saline condition, but no change in controls.

(J) CNO-induced delta (0.5–4 Hz) power increase was significantly larger in DRN^{DA-hM4Di} mice compared to controls ($n = 5$ per group; unpaired t test, ** $p < 0.01$).

(K) CNO-induced high-frequency (40–100 Hz) power decrease was significantly larger in DRN^{DA-hM4Di} mice compared to controls ($n = 5$ per group; unpaired t test, *** $p < 0.0001$).

Data represent mean \pm SEM.

seemingly unrelated roles, valence encoding and sleep-wake regulation, is not unique to midbrain DA groups; wake-promoting LC NA neurons and CRH inputs also convey negative valence (McCall et al., 2015). Considering the involvement of hypocretin and VTA^{DA} systems in reward behavior (España, 2012; Wise, 2004), there may be dichotomous wake-promoting pathways signaling positive or negative valence upon their activation. That DRN^{DA} neurons can simultaneously send arousal and anti-nociceptive signals (Li et al., 2016) can be understood by considering DRN^{DA} connectivity with the bed nucleus of stria terminalis (BNST; Figure S4Q), which is a critical regulator of pain perception (Minami and Ide, 2015).

Compared to ventral midbrain DA counterparts (Schultz, 1997; Ungless et al., 2004; Matsumoto and Hikosaka, 2009; Cohen et al., 2012; Lerner et al., 2015; Kim et al., 2016), the natural dynamics of DRN^{DA} neurons are much less characterized. Due to their relative low number and shared projection targets, DRN^{DA} neurons have been assumed to be functionally similar to VTA^{DA} neurons and hence termed the dorso-caudal extension of the VTA (A10) or A10 dc group (Hokfelt et al., 1984). Several pieces of evidence argue against their treatment as a mere extension of the VTA. Unlike the well-studied dorsal or lateral VTA^{DA} neurons, which fire bursts in response to rewarding or reward-predicting stimuli and are inhibited by punishment (Schultz, 1997; Ungless et al., 2004; Cohen et al., 2012; Kim et al., 2016), or the ventromedial VTA^{DA} neurons, which are selectively excited by aversive stimuli (Brischoux et al., 2009), DRN^{DA} neurons appear to be activated by any alerting or salient stimulus, regardless of valence (Figures 1 and S2). Also, they appear to be minimally affected by physically salient but motivationally neutral cues, such as novel or familiar objects (Figure 1). Since both rewarding and aversive stimuli elicit arousal and motivated responding, the VTA^{DA} system may address this challenge of dual positive (Schultz, 1997) and negative (Brischoux et al., 2009; Matsumoto and Hikosaka, 2009; Zweifel et al., 2011) valence coding in part through segregating to functionally and electrophysiologically distinct subgroups split across anatomical gradients (Brischoux et al., 2009; Bromberg-Martin et al., 2010) or projection targets (Lammel et al., 2011). The DRN^{DA} population, from our observations, showed bimodal activation at the population level, responding to both positive and negative stimuli. Whether individual DRN^{DA} neurons are uniformly excited by positive and negative valence (therefore encoding salience), or whether they are oppositely tuned and intermingled within the DRN, will require future single-cell recording techniques.

DRN^{DA} and VTA^{DA} populations diverge significantly in downstream targets, which may help to explain their functional heterogeneity. Optogenetic excitation of VTA^{DA} neurons, especially those projecting to the nucleus accumbens, supports both appetitive conditioning and positive reinforcement behavior (Wise, 2004; Witten et al., 2011; Steinberg et al., 2014), whereas stimulation of DRN^{DA} neurons produces neutral or mild aversion (Figure S4M; Matthews et al., 2016). These observations may be indicative of differences in downstream connectivity between these neuronal populations. Although DRN^{DA} and VTA^{DA} neurons share overlap in some of their downstream targets (e.g., the prefrontal cortex and the basolateral amygdala), DA neurons projecting to cortical and striatal regions predominantly arise

from the VTA (Björklund and Dunnett, 2007). DRN^{DA} terminals, however, are biased toward the extended amygdala, such as the BNST and central nucleus of the amygdala (CeA) (Figures S4P–S4S; Hasue and Shammah-Lagnado, 2002). Thus, as a major source of excitatory DA drive to the BNST and CeA (Matthews et al., 2016), two regions known to bi-directionally affect motivated behavior and regulate complex emotional states (Jennings et al., 2013), DRN^{DA} neurons are uniquely positioned to provide excitatory signals about environmental salience and internal arousal state to downstream nuclei, which can in turn initiate appropriate behavior, including triggering vigilance or patterning sleep-wake states.

Although DA has been implicated in sleep-wake regulation by pharmacological (Lin et al., 1992), genetic (Wisor et al., 2001), and clinical (Lima, 2013) studies, the precise circuits mediating such actions have been elusive. Single-unit recordings of VTA^{DA} and SNC^{DA} neurons have indicated that they do not change their mean firing rate across distinct sleep-wake states (Miller et al., 1983; Dahan et al., 2007). Here, we show that DRN^{DA} neurons are wake-active (Figures 2 and 3), whereas VTA^{DA} neurons exhibited increased burst firing or Ca²⁺ signals during REM sleep over wakefulness (Dahan et al., 2007; Eban-Rothschild et al., 2016). While the role of VTA^{DA} firing during REM sleep remains elusive, optogenetic activation of VTA^{DA} neurons can promote behavioral and electrocortical arousal (Eban-Rothschild et al., 2016; Taylor et al., 2016). Unlike the DRN^{DA} or VTA^{DA} populations, other DA groups appear to promote sleep rather than wakefulness. For example, chemical lesion of the SNC^{DA} neurons projecting to the dorsal striatum (DS) promotes wakefulness, and optogenetic stimulation of SNC^{DA} terminals in the DS increases NREM sleep (Qiu et al., 2016). Outside the midbrain, A13 zona incerta DA neurons express *c-fos* after REM sleep rebound (Léger et al., 2010). Taken together, these studies indicate that anatomically segregated DA populations may play functionally heterogeneous or even opposing roles in regulating sleep-wake states, and the DRN^{DA} as well as VTA^{DA} systems represent key arousal-promoting DA populations.

As shown here (Figures 6 and S6), external factors can influence sleep-wake patterns, and DRN^{DA} neurons contribute to these processes. Our findings that DRN^{DA} activity tracks the arousal states over broad temporal scales and that DRN^{DA} neurons respond to salient external cues position the DRN^{DA} system at the interface between internal (e.g., wake/sleep drive) and external (e.g., salient stimuli) influences in regulating sleep-wake states. While this evolutionarily conserved trait is advantageous for organism survival, its dysfunction may have negative implications in humans, in which sleep disorders triggered by the malfunctioning of arousal-promoting circuits represent a highly morbid societal burden (Sanford et al., 2015). DRN^{DA} neurons are not well studied in humans, but it has been shown that they degenerate in patients with multiple systems atrophy and Lewy body dementia, which commonly cause excessive daytime sleepiness (Benarroch et al., 2009). Going forward, therapeutic strategies targeting DRN^{DA} activity may have utility in the treatment of primary sleep-wake disorders and sleep/arousal disturbances secondary to myriad neuropsychiatric diseases (Sateia et al., 2000), including major depressive disorder, bipolar affective disorder, and schizophrenia.

STAR★METHODS

Detailed methods are provided in the online version of this paper and include the following:

- KEY RESOURCES TABLE
- CONTACT FOR REAGENT AND RESOURCE SHARING
- EXPERIMENTAL MODEL AND SUBJECT DETAILS
 - Surgeries for viral delivery, optical fiber and EEG/EMG implantation
 - Fiber photometry
 - Behavioral experiments
 - EEG/EMG data acquisition, processing, and sleep-wake state classification
 - Optogenetic and chemogenetic modulation of behavioral states and locomotion
 - Auditory cue arousal test
 - Data analysis
 - Ex vivo electrophysiology
 - Histology
- QUANTIFICATION AND STATISTICAL ANALYSIS

SUPPLEMENTAL INFORMATION

Supplemental Information includes six figures and two movies and can be found with this article online at <http://dx.doi.org/10.1016/j.neuron.2017.05.020>.

AUTHOR CONTRIBUTIONS

J.R.C., J.B.T., and V.G. conceived and designed the project. J.R.C. performed and collected data from EEG/EMG recording, fiber photometry, and optogenetic, chemogenetic, and behavioral experiments. C.X. and J.E.R. performed ex vivo slice recordings. J.R.C., J.B.T., and V.G. analyzed data and made figures. J.R.C. and A.G. assembled the fiber photometry setup and wrote scripts for processing. J.R.C. and L.R.B. set up the EEG and EMG recording system. J.R.C., J.B.T., and V.G. wrote the manuscript with significant contributions from J.E.R. and L.R.B. All authors read and approved the final manuscript. V.G. supervised all aspects of the project.

ACKNOWLEDGMENTS

We would like to acknowledge Drs. Karl Deisseroth and Tom Davidson for the fiber photometry setup. We appreciate the entire Grabiner lab and Dr. David Anderson for helpful discussions. This work was supported by the NIH (Director's New Innovator grants IDP20D017782-01 and PECASE), the NIH/NIA (grants 1R01AG047664-01 and NIH BRAIN 1U01NS090577), the Heritage Medical Research Institute (HMRI-15-09-01), the Pew Charitable Trust (00026171), the Michael J. Fox Foundation (RRIA 2013), Caltech-GIST (CG2013), and the Sloan Foundation (FR2015-65471, to V.G.). J.B.T. is a Colvin postdoctoral fellow. J.E.R. is supported by the Children's Tumor Foundation (2016-01-006). C.X. was partly supported by the Michael J. Fox Foundation.

Received: October 6, 2016

Revised: March 31, 2017

Accepted: May 11, 2017

Published: June 8, 2017

REFERENCES

- Aston-Jones, G., and Bloom, F.E. (1981). Activity of norepinephrine-containing locus coeruleus neurons in behaving rats anticipates fluctuations in the sleep-waking cycle. *J. Neurosci.* 1, 876–886.
- Benarroch, E.E., Schmeichel, A.M., Dugger, B.N., Sandroni, P., Parisi, J.E., and Low, P.A. (2009). Dopamine cell loss in the periaqueductal gray in multiple system atrophy and Lewy body dementia. *Neurology* 73, 106–112.
- Björklund, A., and Dunnett, S.B. (2007). Dopamine neuron systems in the brain: an update. *Trends Neurosci.* 30, 194–202.
- Brischoux, F., Chakraborty, S., Brierley, D.I., and Ungless, M.A. (2009). Phasic excitation of dopamine neurons in ventral VTA by noxious stimuli. *Proc. Natl. Acad. Sci. USA* 106, 4894–4899.
- Bromberg-Martin, E.S., Matsumoto, M., and Hikosaka, O. (2010). Dopamine in motivational control: rewarding, aversive, and alerting. *Neuron* 68, 815–834.
- Brown, R.E., Basheer, R., McKenna, J.T., Strecker, R.E., and McCarley, R.W. (2012). Control of sleep and wakefulness. *Physiol. Rev.* 92, 1087–1187.
- Chen, T.W., Wardill, T.J., Sun, Y., Pulver, S.R., Renninger, S.L., Baohan, A., Schreiter, E.R., Kerr, R.A., Orger, M.B., Jayaraman, V., et al. (2013). Ultrasensitive fluorescent proteins for imaging neuronal activity. *Nature* 499, 295–300.
- Cohen, J.Y., Haesler, S., Vong, L., Lowell, B.B., and Uchida, N. (2012). Neuron-type-specific signals for reward and punishment in the ventral tegmental area. *Nature* 482, 85–88.
- Daberkow, D.P., Brown, H.D., Bunner, K.D., Kraniotis, S.A., Doellman, M.A., Ragozzino, M.E., Garris, P.A., and Roitman, M.F. (2013). Amphetamine paradoxically augments exocytotic dopamine release and phasic dopamine signals. *J. Neurosci.* 33, 452–463.
- Dahan, L., Astier, B., Vautrelle, N., Urbain, N., Kocsis, B., and Chouvet, G. (2007). Prominent burst firing of dopaminergic neurons in the ventral tegmental area during paradoxical sleep. *Neuropsychopharmacology* 32, 1232–1241.
- Descarries, L., Berthelet, F., Garcia, S., and Beaudet, A. (1986). Dopaminergic projection from nucleus raphe dorsalis to neostriatum in the rat. *J. Comp. Neurol.* 249, 511–520, 484–515.
- Dougalis, A.G., Matthews, G.A., Bishop, M.W., Brischoux, F., Kobayashi, K., and Ungless, M.A. (2012). Functional properties of dopamine neurons and co-expression of vasoactive intestinal polypeptide in the dorsal raphe nucleus and ventro-lateral periaqueductal grey. *Eur. J. Neurosci.* 36, 3322–3332.
- Eban-Rothschild, A., Rothschild, G., Giardino, W.J., Jones, J.R., and de Lecea, L. (2016). VTA dopaminergic neurons regulate ethologically relevant sleep-wake behaviors. *Nat. Neurosci.* 19, 1356–1366.
- España, R.A. (2012). Hypocretin/orexin involvement in reward and reinforcement. *Vitam. Horm.* 89, 185–208.
- Garey, J., Goodwillie, A., Frohlich, J., Morgan, M., Gustafsson, J.A., Smithies, O., Korach, K.S., Ogawa, S., and Pfaff, D.W. (2003). Genetic contributions to generalized arousal of brain and behavior. *Proc. Natl. Acad. Sci. USA* 100, 11019–11022.
- George, E.D., Bordner, K.A., Elwafi, H.M., and Simen, A.A. (2010). Maternal separation with early weaning: a novel mouse model of early life neglect. *BMC Neurosci.* 11, 123.
- Gjerstad, M.D., Wentzel-Larsen, T., Aarsland, D., and Larsen, J.P. (2007). Insomnia in Parkinson's disease: frequency and progression over time. *J. Neurol. Neurosurg. Psychiatry* 78, 476–479.
- Gunaydin, L.A., Grosenick, L., Finkelstein, J.C., Kauvar, I.V., Fenno, L.E., Adhikari, A., Lammel, S., Mirzabekov, J.J., Airan, R.D., Zalociusky, K.A., et al. (2014). Natural neural projection dynamics underlying social behavior. *Cell* 157, 1535–1551.
- Hasue, R.H., and Shammah-Lagnado, S.J. (2002). Origin of the dopaminergic innervation of the central extended amygdala and accumbens shell: a combined retrograde tracing and immunohistochemical study in the rat. *J. Comp. Neurol.* 454, 15–33.
- Hokfelt, T., Martensson, R., Björklund, A., Kleinau, S., and Goldstein, M. (1984). Distribution Maps of Tyrosine-Hydroxylase-Immunoreactive Neurons in the Rat Brain (Elsevier).
- Jennings, J.H., Sparta, D.R., Stamatakis, A.M., Ung, R.L., Pleil, K.E., Kash, T.L., and Stuber, G.D. (2013). Distinct extended amygdala circuits for divergent motivational states. *Nature* 496, 224–228.

- Jones, B.E. (1991). Paradoxical sleep and its chemical/structural substrates in the brain. *Neuroscience* 40, 637–656.
- Jouvet, M. (1999). Sleep and serotonin: an unfinished story. *Neuropsychopharmacology* 21 (2, Suppl), 24S–27S.
- Kim, C.K., Yang, S.J., Pichamoorthy, N., Young, N.P., Kauvar, I., Jennings, J.H., Lerner, T.N., Berndt, A., Lee, S.Y., Ramakrishnan, C., et al. (2016). Simultaneous fast measurement of circuit dynamics at multiple sites across the mammalian brain. *Nat. Methods* 13, 325–328.
- Lammel, S., Ion, D.I., Roepke, J., and Malenka, R.C. (2011). Projection-specific modulation of dopamine neuron synapses by aversive and rewarding stimuli. *Neuron* 70, 855–862.
- Lammel, S., Lim, B.K., Ran, C., Huang, K.W., Betley, M.J., Tye, K.M., Deisseroth, K., and Malenka, R.C. (2012). Input-specific control of reward and aversion in the ventral tegmental area. *Nature* 491, 212–217.
- Lammel, S., Lim, B.K., and Malenka, R.C. (2014). Reward and aversion in a heterogeneous midbrain dopamine system. *Neuropharmacology* 76 (Pt B), 351–359.
- Léger, L., Sapin, E., Goutagny, R., Peyron, C., Salvert, D., Fort, P., and Luppi, P.H. (2010). Dopaminergic neurons expressing Fos during waking and paradoxical sleep in the rat. *J. Chem. Neuroanat.* 39, 262–271.
- Lerner, T.N., Shlyansky, C., Davidson, T.J., Evans, K.E., Beier, K.T., Zalocusky, K.A., Crow, A.K., Malenka, R.C., Luo, L., Tomer, R., and Deisseroth, K. (2015). Intact-brain analyses reveal distinct information carried by SNc dopamine subcircuits. *Cell* 162, 635–647.
- Li, C., Sugam, J.A., Lowery-Gionta, E.G., McElligott, Z.A., McCall, N.M., Lopez, A.J., McKiernan, J.M., Pleil, K.E., and Kash, T.L. (2016). Mu opioid receptor modulation of dopamine neurons in the periaqueductal gray/dorsal raphe: a role in regulation of pain. *Neuropsychopharmacology* 41, 2122–2132.
- Lima, M.M. (2013). Sleep disturbances in Parkinson's disease: the contribution of dopamine in REM sleep regulation. *Sleep Med. Rev.* 17, 367–375.
- Lin, J.S., Roussel, B., Akaoka, H., Fort, P., Debilly, G., and Jouvet, M. (1992). Role of catecholamines in the modafinil and amphetamine induced wakefulness, a comparative pharmacological study in the cat. *Brain Res.* 591, 319–326.
- Lu, J., Jhou, T.C., and Saper, C.B. (2006). Identification of wake-active dopaminergic neurons in the ventral periaqueductal gray matter. *J. Neurosci.* 26, 193–202.
- Margolis, E.B., Mitchell, J.M., Ishikawa, J., Hjelmstad, G.O., and Fields, H.L. (2008). Midbrain dopamine neurons: projection target determines action potential duration and dopamine D(2) receptor inhibition. *J. Neurosci.* 28, 8908–8913.
- Matsumoto, M., and Hikosaka, O. (2009). Two types of dopamine neuron distinctly convey positive and negative motivational signals. *Nature* 459, 837–841.
- Matthews, G.A., Nieh, E.H., Vander Weele, C.M., Halbert, S.A., Pradhan, R.V., Yosafat, A.S., Globor, G.F., Izadmehr, E.M., Thomas, R.E., Lacy, G.D., et al. (2016). Dorsal raphe dopamine neurons represent the experience of social isolation. *Cell* 164, 617–631.
- Mattis, J., Tye, K.M., Ferenczi, E.A., Ramakrishnan, C., O'Shea, D.J., Prakash, R., Gunaydin, L.A., Hyun, M., Fenno, L.E., Grdinariu, V., et al. (2011). Principles for applying optogenetic tools derived from direct comparative analysis of microbial opsins. *Nat. Methods* 9, 159–172.
- McCall, J.G., Al-Hasani, R., Siuda, E.R., Hong, D.Y., Norris, A.J., Ford, C.P., and Bruchas, M.R. (2015). CRH engagement of the locus coeruleus noradrenergic system mediates stress-induced anxiety. *Neuron* 87, 605–620.
- McDevitt, R.A., Tiran-Cappello, A., Shen, H., Balderas, I., Britt, J.P., Marino, R.A., Chung, S.L., Richie, C.T., Harvey, B.K., and Bonci, A. (2014). Serotonergic versus nonserotonergic dorsal raphe projection neurons: differential participation in reward circuitry. *Cell Rep.* 8, 1857–1869.
- Miller, J.D., Farber, J., Gatz, P., Roffwarg, H., and German, D.C. (1983). Activity of mesencephalic dopamine and non-dopamine neurons across stages of sleep and walking in the rat. *Brain Res.* 273, 133–141.
- Minami, M., and Ide, S. (2015). How does pain induce negative emotion? Role of the bed nucleus of the stria terminalis in pain-induced place aversion. *Curr. Mol. Med.* 15, 184–190.
- Morales, M., and Margolis, E.B. (2017). Ventral tegmental area: cellular heterogeneity, connectivity and behaviour. *Nat. Rev. Neurosci.* 18, 73–85.
- Nagatsu, I., Inagaki, S., Kondo, Y., Karasawa, N., and Nagatsu, T. (1979). Immunofluorescent studies on the localization of tyrosine hydroxylase and dopamine-beta-hydroxylase in the mes-, di-, and telencephalon of the rat using unperfused fresh frozen section. *Acta Histochem. Cytochem.* 12, 20–37.
- Pimentel, D., Donlea, J.M., Talbot, C.B., Song, S.M., Thurston, A.J., and Miesenböck, G. (2016). Operation of a homeostatic sleep switch. *Nature* 536, 333–337.
- Pinto, L., Goard, M.J., Estandian, D., Xu, M., Kwan, A.C., Lee, S.H., Harrison, T.C., Feng, G., and Dan, Y. (2013). Fast modulation of visual perception by basal forebrain cholinergic neurons. *Nat. Neurosci.* 16, 1857–1863.
- Poulin, J.F., Zou, J., Drouin-Ouellet, J., Kim, K.Y., Cicchetti, F., and Awatramani, R.B. (2014). Defining midbrain dopaminergic neuron diversity by single-cell gene expression profiling. *Cell Rep.* 9, 930–943.
- Qiu, M.H., Yao, Q.L., Vetrivelan, R., Chen, M.C., and Lu, J. (2016). Nigrostriatal dopamine action on globus pallidus regulates sleep. *Cereb. Cortex* 26, 1430–1439.
- Qu, W.M., Huang, Z.L., Xu, X.H., Matsumoto, N., and Urade, Y. (2008). Dopaminergic D1 and D2 receptors are essential for the arousal effect of modafinil. *J. Neurosci.* 28, 8462–8469.
- Rajasethupathy, P., Ferenczi, E., and Deisseroth, K. (2016). Targeting neural circuits. *Cell* 165, 524–534.
- Sakurai, T., Amemiya, A., Ishii, M., Matsuzaki, I., Chemelli, R.M., Tanaka, H., Williams, S.C., Richardson, J.A., Kozlowski, G.P., Wilson, S., et al. (1998). Orexins and orexin receptors: a family of hypothalamic neuropeptides and G protein-coupled receptors that regulate feeding behavior. *Cell* 92, 573–585.
- Sanford, L.D., Suchecki, D., and Meerlo, P. (2015). Stress, arousal, and sleep. *Curr. Top. Behav. Neurosci.* 25, 379–410.
- Sateia, M.J., Greenough, G., and Nowell, P. (2000). Sleep in neuropsychiatric disorders. *Semin. Clin. Neuropsychiatry* 5, 227–237.
- Schultz, W. (1997). Dopamine neurons and their role in reward mechanisms. *Curr. Opin. Neurobiol.* 7, 191–197.
- Schweimer, J.V., and Ungless, M.A. (2010). Phasic responses in dorsal raphe serotonin neurons to noxious stimuli. *Neuroscience* 171, 1209–1215.
- Steinberg, E.E., Boivin, J.R., Saunders, B.T., Witten, I.B., Deisseroth, K., and Janak, P.H. (2014). Positive reinforcement mediated by midbrain dopamine neurons requires D1 and D2 receptor activation in the nucleus accumbens. *PLoS ONE* 9, e94771.
- Szymusiak, R., and McGinty, D. (2008). Hypothalamic regulation of sleep and arousal. *Ann. N Y Acad. Sci.* 1129, 275–286.
- Takahashi, K., Kayama, Y., Lin, J.S., and Sakai, K. (2010). Locus coeruleus neuronal activity during the sleep-waking cycle in mice. *Neuroscience* 169, 1115–1126.
- Taylor, N.E., Van Dort, C.J., Kenny, J.D., Pei, J., Guidera, J.A., Vlasov, K.Y., Lee, J.T., Boyden, E.S., Brown, E.N., and Solt, K. (2016). Optogenetic activation of dopamine neurons in the ventral tegmental area induces reanimation from general anesthesia. *Proc. Natl. Acad. Sci. USA* 113, 12826–12831.
- Tsai, H.C., Zhang, F., Adamantidis, A., Stuber, G.D., Bonci, A., de Lecea, L., and Deisseroth, K. (2009). Phasic firing in dopaminergic neurons is sufficient for behavioral conditioning. *Science* 324, 1080–1084.
- Ungless, M.A., Magill, P.J., and Bolam, J.P. (2004). Uniform inhibition of dopamine neurons in the ventral tegmental area by aversive stimuli. *Science* 303, 2040–2042.

- Urban, D.J., and Roth, B.L. (2015). DREADDs (designer receptors exclusively activated by designer drugs): chemogenetic tools with therapeutic utility. *Annu. Rev. Pharmacol. Toxicol.* 55, 399–417.
- Vinck, M., Batista-Brito, R., Knoblich, U., and Cardin, J.A. (2015). Arousal and locomotion make distinct contributions to cortical activity patterns and visual encoding. *Neuron* 86, 740–754.
- Whitaker, L.R., Degoulet, M., and Morikawa, H. (2013). Social deprivation enhances VTA synaptic plasticity and drug-induced contextual learning. *Neuron* 77, 335–345.
- Winsky-Sommerer, R., Boutrel, B., and de Lecea, L. (2005). Stress and arousal: the corticotrophin-releasing factor/hypocretin circuitry. *Mol. Neurobiol.* 32, 285–294.
- Wise, R.A. (2004). Dopamine, learning and motivation. *Nat. Rev. Neurosci.* 5, 483–494.
- Wisor, J.P., Nishino, S., Sora, I., Uhl, G.H., Mignot, E., and Edgar, D.M. (2001). Dopaminergic role in stimulant-induced wakefulness. *J. Neurosci.* 21, 1787–1794.
- Witten, I.B., Steinberg, E.E., Lee, S.Y., Davidson, T.J., Zalocusky, K.A., Brodsky, M., Yizhar, O., Cho, S.L., Gong, S., Ramakrishnan, C., et al. (2011). Recombinase-driver rat lines: tools, techniques, and optogenetic application to dopamine-mediated reinforcement. *Neuron* 72, 721–733.
- Xu, M., Chung, S., Zhang, S., Zhong, P., Ma, C., Chang, W.C., Weissbourd, B., Sakai, N., Luo, L., Nishino, S., and Dan, Y. (2015). Basal forebrain circuit for sleep-wake control. *Nat. Neurosci.* 18, 1641–1647.
- Zweifel, L.S., Fadok, J.P., Argilli, E., Garelick, M.G., Jones, G.L., Dickerson, T.M., Allen, J.M., Mizumori, S.J., Bonci, A., and Palmiter, R.D. (2011). Activation of dopamine neurons is critical for aversive conditioning and prevention of generalized anxiety. *Nat. Neurosci.* 14, 620–626.

STAR★METHODS**KEY RESOURCES TABLE**

REAGENT or RESOURCE	SOURCE	IDENTIFIER
Antibodies		
Chicken polyclonal anti-TH	Aves Labs	Cat#: TYH RRID: AB_10013440
Rabbit polyclonal anti-TH	Santa Cruz	Cat#: sc-14007 RRID: AB_671397
Chicken polyclonal anti-GFP	Aves Labs	Cat#: GFP-1020 RRID: AB_10000240
Goat polyclonal anti-5HT	Immunostar	Cat#: 20079 RRID: AB_572262
Rabbit polyclonal anti-mCherry	Abcam	Cat#: ab167453 RRID: AB_2571870
Anti-chicken Alexa Fluor 488	Jackson ImmunoResearch	Cat#: 703-545-155 RRID: AB_2340375
Anti-rabbit Alexa Fluor 488	Jackson ImmunoResearch	Cat#: 711-545-152 RRID: AB_2313584
Anti-goat Rhodamine Red-X	Jackson ImmunoResearch	Cat#: 705-297-003 RRID: AB_2340425
Anti-rabbit Rhodamine Red-X	Jackson ImmunoResearch	Cat#: 711-297-003 RRID: AB_2340615
Anti-rabbit Alexa Fluor 647	Jackson ImmunoResearch	Cat#: 711-607-003 RRID: AB_2340626
Anti-chicken Alexa Fluor 647	Jackson ImmunoResearch	Cat#: 703-606-155 RRID: AB_2340380
Chemicals, Peptides, and Recombinant Proteins		
Clozapine-N-oxide	Enzo Life Science	Cat#: BML-NS105
Experimental Models: Organisms/Strains		
Mouse: TH::IRES-Cre	European Mouse Mutant Archive	EM: 00254
Recombinant DNA		
AAV5-Syn-FLEX-GCaMP6f	Penn Vector Core	AV-5-PV2819
AAV5-Syn-FLEX-GCaMP6s	Penn Vector Core	AV-5-PV2821
AAV5-Ef1a-DIO-ChR2(H134R)-eYFP	UNC Vector Core	N/A
AAV5-Ef1a-DIO-eArch3.0-eYFP	UNC Vector Core	N/A
AAV5-hSyn-DIO-EGFP	UNC Vector Core	N/A
AAV2-hSyn-DIO-hM4Di-mCherry	UNC Vector Core/Addgene	N/A
Software and Algorithms		
MATLAB R2014a	Mathworks	N/A
pClamp 10.4	Molecular Devices	N/A
SleepSign 3.0	Kissei Comtec	N/A
EthoVision XT10	Noldus Information Technology	N/A
ABETII	Lafayette Instrument	N/A
Prism 5.0	GraphPad Software	N/A

CONTACT FOR REAGENT AND RESOURCE SHARING

Detailed information and requests for agents may be directed to and will be fulfilled by the Lead Contact, Viviana Gradinaru (viviana@caltech.edu).

EXPERIMENTAL MODEL AND SUBJECT DETAILS

Tyrosine hydroxylase (TH)::IRES-Cre knockin mice were obtained from the European Mouse Mutant Archive (EM::00254) and crossed with wild-type C57BL/6N mice. We exclusively used male heterozygote mice for fiber photometry during behaviors and used both male and female heterozygote mice for other experiments with EEG/EMG. After weaning, animals were group-housed until they were 3–4 months old. Upon the completion of any surgical procedures, mice were allowed to recover from anesthesia on a heating-pad, and then they were transferred, singly housed (or group-housed for the group-housed cohort) to a new residence room for full recovery (2–4 weeks) prior to the start of any behavioral experiments or habituation to EEG/EMG tethers. In this

residence/procedure room, subjects were housed on a 12 h: 12 hr light/dark cycle (light off at 6AM, light on at 6PM) with ad libitum access to food and water. Animal husbandry and all experimental procedures involving animal subjects were approved by the Institutional Animal Care and Use Committee (IACUC) and by the Office of Laboratory Animal Resources at the California Institute of Technology under IACUC protocol 1672.

Surgeries for viral delivery, optical fiber and EEG/EMG implantation

General surgical procedures and viral delivery

Mice were anesthetized with isoflurane gas/carbogen mixture (5% for induction and 1.5%–2% for maintenance during surgery) and placed to a stereotaxic frame (David Kopf Instruments, CA, USA). After shaving their hair and sterilizing the skin with chlorohexidine, a midline incision was made with a sterile scalpel. The skull surface was wiped and cleaned with autoclaved cotton swabs. Bregma and lambda were identified and leveled to be on the same z axis. Small craniotomy holes were made for 20 degree angled injection of viruses and optical fiber implantation over the dorsal raphe nucleus (DRN, antero-posterior (AP) axis: –4.65 mm, medio-lateral (ML) axis: ± 1.2 mm, relative to Bregma). Adeno-associated viral vectors (AAV, see below for details) were injected into the DRN (AP –4.6 mm, ML ± 1.2 mm, dorso-ventral (DV) –2.95 mm, at a 20 degree angle relative to vertical axis from the left and right sides). Viral injection was performed using a blunt 35-gauge microinjection needle within a 10 μ L microsyringe (NanoFil, World Precision Instruments, FL, USA), which was controlled by a microsyringe pump (UMP3, World Precision Instruments) connected to a controller (Micro4, World Precision Instruments). 0.3–0.5 μ L of AAV was infused per site at a rate of 50 nL per min. Following injection, the needle/syringe was held in the same location for an additional 10 min to allow further diffusion. To prevent potential backflow, the needle/syringe was slowly withdrawn over approximately 10 min.

EEG and EMG implantation

To implant the EEG/EMG apparatus, three additional craniotomy holes were made in frontal (for first EEG channel; AP +2.0 mm, ML +0.7 mm), central (for second EEG channel; AP –1.3 mm, ML +1.3 mm) and lateral parietal (for reference and ground; AP –3.5 mm, ML –2.5 mm) regions with a drill bit (#73, 105-0240.340, Kyocera, Kyoto, Japan). 0.10" electrodes with wire leads (8403, Pinnacle Technology Inc., KS, USA) were screwed into the craniotomy holes. With the leads from the screw electrodes held away from the surface of the skull to prevent accidental glue application, a thin layer of adhesive cement (C&B Metabond, Parkell Inc., NY, USA) was applied on the skull surface to secure the screw electrodes. Another thin layer of dental cement (51458, Stoelting Co., IL, USA) was additionally applied until it covered screw heads. The EEG/EMG headmount (8201, Pinnacle Technology Inc.) was then placed on the dental cement layer and lead wires from screw electrodes were connected to the headmount. Silver epoxy (MG Chemicals, BC, Canada) was applied to ensure electrical conduction between the lead wires and headmount. An additional layer of dental cement was applied to secure the headmount to the animal's head. Finally, EMG leads from the headmount were inserted into the trapezius muscles and then the incision was closed.

Optical fiber implantation (for fiber photometry and optogenetic experiments)

Following virus infusion, an optical ferrule/fiber with cut length of 4 mm and diameter of 300 μ m (for optogenetics, NA 0.37, home-made) or 400 μ m (for fiber photometry, NA 0.48, Doric lenses, Quebec, QC, Canada) was firmly mounted to a stereotaxic holder (1766AP, David Kopf Instruments, CA, USA). An optical ferrule/fiber was then inserted to the DRN (AP –4.6 mm, ML ± 1.2 mm, DV –2.5~2.7 mm, at a 20 degree angle relative to vertical axis from either left or right side) through a craniotomy hole, and stopped 200 (for fiber photometry) or 500 μ m (for optogenetics) above the viral injection site. A thin layer of adhesive cement was applied on the skull surface to strongly hold the ferrule/fiber. After adhesive cement was completely dried, a thick layer of pink dental cement was applied to build a robust head cap.

Viral constructs

For fiber photometry experiments, 0.5 μ L of AAV serotype 5 encoding GCaMP6f or GCaMP6s (Chen et al., 2013) under synapsin promoter and Cre-dependent FLEX switch (AAV5-Syn-FLEX-GCaMP6f or GCaMP6s, 1.0–1.5 $\times 10^{13}$ genome copies/mL) was unilaterally injected. GCaMP6 viruses were packaged and purchased from the University of Pennsylvania Vector Core (Philadelphia, PA, USA). For optogenetic activation experiments, 0.3 μ L of AAV serotype 5 encoding ChR2-eYFP under Ef1a promoter and double-floxed inverse open reading frame (DIO) (AAV5-Ef1a-DIO-ChR2(h134R)-eYFP, 4.5 $\times 10^{12}$ genome copies/mL) was bilaterally injected. For chemogenetic experiments, 0.3 μ L of AAV serotype 2 encoding hM4Di-mCherry under human synapsin promoter and DIO switch (AAV2-hSyn-DIO-hM4Di-mCherry, 4.0 – 5.0 $\times 10^{12}$ genome copies/mL) was bilaterally injected. For optogenetic inhibition experiments, 0.5 μ L of AAV serotype 5 encoding eArch3.0-eYFP under Ef1a promoter and DIO frame (AAV5-Ef1a-DIO-eArch3.0-eYFP, 3.4 $\times 10^{12}$ genome copies/mL) was bilaterally injected. For control animals, 0.5 μ L of AAV5-hSyn-DIO-eGFP (4.7 $\times 10^{12}$ genome copies/mL) was bilaterally injected. ChR2-eYFP, hM4Di-mCherry, eArch3.0-eYFP and eGFP viruses were packaged and purchased from the University of North Carolina Vector Core (Chapel Hill, NC, USA). hM4Di-mCherry vector was also purchased from Addgene (Cambridge, MA, USA).

Fiber photometry

Fiber photometry is a method of measuring population Ca^{2+} sensitive fluorescence from genetically defined cell types in deep brain structures, such as TH-expressing neurons in the DRN, using a single optical fiber for both excitation and emission in freely moving mice (Gunaydin et al., 2014). We based our photometry design from a previous literature (Lerner et al., 2015) with a few modifications. Two wavelength LEDs (490 nm for GCaMP6 excitation and 405 nm for isosbestic wavelength excitation, M490F1 and M405F1,

Thorlabs Inc., NJ, USA) were modulated at two different frequencies (211 Hz for 490 nm, 531 Hz for 405 nm), which were controlled by a real-time processor (RX8-2, Tucker David Technologies, FL, USA) and a custom-written software (provided by Drs. Karl Deisseroth and Tom Davidson at Stanford University). The emission signal from 405 nm illumination was shown to be Ca^{2+} -independent with GCaMP6 and to mostly reflect bleaching and motion artifacts (Lerner et al., 2015; Kim et al., 2016): thus, this signal serves as a control reference signal. 490 nm and 405 nm excitation lights were passed through GFP and violet cleanup excitation filters (FF02-472/30-25 and FF01-400/40-25, Semrock, NY, USA) respectively, and reflected off dichroic mirrors (DMLP425 and MD498, Thorlabs). Excitation light was coupled into a low auto-fluorescence 400 μm patch cord (0.48 NA, 2 m cable length, Doric lenses) with a high NA coupler/collimator (F240FC-A, Thorlabs). Another end of the patch cord was connected to a ceramic optical ferrule/fiber (1.25 mm diameter ferrule, 400 μm diameter fiber core) implanted into the brain region of interest in subjects. The LED powers for both excitation wavelengths were measured with a power meter (PM100D, Thorlabs) and set to be 50–80 μW at the end of the patch cord. GCaMP6 emission signals were collected through the patch cord and collimator and passed through a dichroic mirror (MD498, Thorlabs) and a GFP emission filter (MF525-39, Thorlabs) to reach a femtowatt photoreceiver (Model 2151, Newport Co., Irvine, CA, USA) using a focusing lens (62-561, Edmunds Optics, Barrington, NJ, USA). Photoreceiver signals were relayed into a RX8-2 processor through a BNC cable and were demodulated into two signals, corresponding to each LED excitation wavelength based on its modulation frequency. These outputs were digitized at a sampling rate of 382 Hz and low-pass filtered at 15 Hz. One digital input channel was additionally acquired to record any TTL pulses from an external source in order to synchronize transients with EEG/EMG, video recording, and/or behavioral events. Custom-written software was used to control data acquisition and signal visualization.

Behavioral experiments

All behavioral experiments involving fiber photometry were performed at least 2 weeks after viral injection. Behavioral tests with optogenetics were performed at least 4 weeks after surgery to allow maximal transgene expression. Mice underwent the following assays during their dark phase (10AM–5PM) in their residence room, unless otherwise stated.

Resident-intruder assay

Mice with an implanted optical fiber were connected to a patch cord for recording of fiber photometry. After connection, mice were placed back into their home cages and habituated to the open cage setup for 10 min. After habituation, a juvenile male (3–4 weeks old), adult female (2–3 months old), or adult male (2–3 months old) mouse was introduced as an intruder into each home cage. Video recording was performed and synchronized with fiber photometry signals. After 5 min, the intruder mouse was removed from the home cage. The behavior of resident mice, such as investigation and attack (observed only toward adult males), was manually scored by an experimenter.

Novel object interaction assay

The novel object interaction test setup was almost identical to the resident-intruder assay, but a distinct novel object was placed into the center of the empty cages instead of an intruder mouse. To run the test, mice were connected to the photometry patch cord, and habituated to being tethered in the open empty cage environment. Then, a novel object was introduced, and the subject was allowed to freely explore the object for a 5 min test session. Behavior scoring was manually performed to identify interaction bouts, which consisted of the subject approaching, sniffing, and/or touching of the object with forelimbs.

Familiar object interaction assay

This assay was similar to the novel object interaction assay described above, except that the designated familiar object (similar size and characteristics as used for the novel objects) was placed into the subject's home cage 5 days prior to photometry recording sessions.

Feeding assay

Two days before the experiment, the palatable food treat (approximately 1 g of peanut butter chocolate pieces (Reese's peanut butter cups)) was presented to each mouse for consumption. After connecting the mouse to the patch cord, they were placed in a clean, empty cage. After 5 min of habituation, approximately 2 g of treats in a small weighing boat were introduced into one of the cage corners. All tested subjects approached and consumed the treat after variable delays. Leftover treats were removed after 10 min. Video recordings were manually scored to identify food consumption bouts.

Air puff

Mice were connected to a patch cord and placed in a clean empty cage without any bedding. Mice were allowed to explore and habituate for 5 min. Six brief (< 1 s) air puffs were applied to the tail using a compressed air duster with an inter-puff interval of 30–60 s. TTL pulses were sent to the fiber photometry digital input channel for time stamping when air puffs were applied.

Unpredictable delivery of electric footshocks

Mice were connected to a patch cord and placed inside an operant chamber (Lafayette Instruments, IN, USA). Mice were allowed to explore and habituate to the operant box for 10 min. Two mild footshocks (0.3 mA, 1 s) were delivered with intervals of about 30 s. TTL pulses were sent to the fiber photometry digital input channel for accurate time stamping.

Exposure to predator odor

Mice were connected to a patch cord and moved to a clean empty cage. To habituate to this new environment, mice were allowed to explore for 5 min. After photometry recording started, a filter paper applied with 10 μ L of 2,3,5-trimethyl-3-thiazoline (TMT, a component of fox urine, SRQ Bio, Inc, FL, USA) was introduced to the cage corner. Simultaneous photometry and video recordings were performed to identify the time point of odor investigation.

Restraint/Immobilization

A test subject was connected to a patch cord and placed to a clean empty cage. A 5 min habituation session was conducted in which the subject was allowed to freely explore the cage. At the start of fiber photometry recording, 3 min of baseline data were obtained. Then, taking care not to cause significant pain to the subject, a trained experimenter restrained the subject for one minute by placing gentle pressure on the mouse body with the left hand and immobilizing the tail with the right hand. All subjects engaged in active struggling and escape behaviors. Recordings were terminated after 3 min of recovery.

Tail suspension test

Mice were connected to a patch cord, and the tail was placed between strips of common lab tape, which was affixed to a horizontal bar suspended about 50 cm from the ground. We additionally put a lightweight (~1 g) plastic cylinder around the tail to prevent the mouse from climbing onto the tail. Synchronized fiber photometry and video recordings were performed for 5 min, and video was manually and blindly scored to pinpoint “mobility” bouts during which the animals struggled by moving their bodies.

Open field test

Mice were connected to a patch cord, transferred to the open field box (50 cm x 50 cm x 25 cm), and habituated to this setup for 10-15 min prior to the start of 15 min test sessions. A video camera positioned above the behavioral arena and connected to EthoVision XT 9 software (Noldus Information Technology, Wageningen, Netherlands) allowed tracking of subject position and velocity throughout the test session. Fiber photometry and video recordings were synchronized via TTL pulses generated by the Noldus USB-IO box. Fiber photometry experiments took place during the subjects' dark phase (10AM-5PM). For optogenetic experiments, open field tests were performed during both the dark phase (9AM-1PM) and light phase (6PM-10PM) to examine whether locomotion varied across the circadian cycle. The order of open field test sessions during dark and light phases was counter-balanced.

Real-time place preference/aversion assay

A subject was connected to a patch cord and transferred to the open field box (50 cm x 25 cm x 25 cm), which was divided into left and right compartments. The subject was given free access to explore the two compartments for 30 min. However, upon entering the “paired chamber,” the subject received phasic bursts of optogenetic stimulation (30 Hz, 10 pulses, 10 ms pulse width, every 5 s). The side paired with optogenetic stimulation was counter-balanced. EthoVision XT 9 software (Noldus) was used to track the movement and location of mice. As a dependent variable, time spent in the paired compartment was quantified.

EEG/EMG data acquisition, processing, and sleep-wake state classification

After EEG/EMG implantation surgery, animals were single-housed for four weeks in a regular mouse cage for recovery and transgene expression. Mice were then transferred to a transparent cylindrical cage (12" diameter and 12" height) and connected to a customized pre-amplifier (10x gain, 0.5 Hz high-pass filter, 10 Hz high-pass filter for EMG; Pinnacle Technology Inc., Lawrence, KS, USA) and a commutator (8204, Pinnacle Technology Inc.) for freely moving recordings. They were habituated for at least seven days to the recording setup before beginning any experiments. On the 7th day, four animals were randomly selected per group (depending on the viral transgene they expressed) and 24 hr baseline recordings were performed to test whether viral transgene expression or other experimental artifacts altered the sleep-wake architecture of subjects. Food and water were available ad libitum. EEG/EMG signals were digitized through the OmniPlex System (Plexon, TX, USA) with a sampling rate of 1,000 Hz in most experiments, or through Pinnacle Sirenia Acquisition (Pinnacle Technology Inc, KS, USA) with a sampling rate of 400 Hz (for 24 hr baseline recordings and chemogenetic experiments in presence of salient stimuli). Mice with lost EEG and EMG signals were excluded from the experiment - very occasionally, some mice showed a low signal-to-noise ratio or unintelligible EEG/EMG traces.

Data acquired in Plexon's or Pinnacle's proprietary file format (.pl2 or .pvfs) were converted to European data format (.edf) with MATLAB (MathWorks, MA, USA) using the EEGLAB plug-in (Schwartz Center for Computational Neuroscience, La Jolla, CA, USA). Polysomnographic EEG/EMG recordings were loaded, and behavioral states were scored using sleep analysis software (SleepSign for Animal, Kissei Comtec Co., Nagano, Japan).

Sleep-wake state classification is manually performed based on visual and spectral signatures of EEG and EMG signals. States were assigned across consecutive non-overlapping 5 s windows. We defined wakefulness as desynchronized, low-amplitude, and high-frequency EEG rhythms with elevated EMG activity. We defined NREM sleep as synchronized, high-amplitude, and low-frequency (< 4 Hz) EEG activity with lower tonic EMG tone. We defined REM sleep as containing prominent theta (6-10 Hz) oscillations on EEG and minimal EMG activity. All sleep-wake state scorings were performed by an experimenter (J.R.C.), who was blind to expressed transgene and experimental conditions.

Optogenetic and chemogenetic modulation of behavioral states and locomotion

For optogenetic experiments, one side of a patch cord (1.25 mm ceramic ferrule, 300 μ m diameter, Doric lenses) was connected to the implanted optical ferrule/fiber with another side (FC/PC connector) connected to a swivel commutator (fiber-optic rotary joints,

FRJ_1x1_FC-FC, Doric lenses) to allow free movement. Another patch cord was connected from the commutator to a 473 nm laser (MLL-FN-473nm/150mW, Changchun New Industries Optoelectronics Technology, Changchun, China). The intensity of the laser beam was measured with an optical power meter (PM100D, Thorlabs) and set to be 10 mW at the tip. Laser output was controlled by a TTL pulse generator (OTPG4, Doric lenses) via a BNC cable. For phasic stimulation, ten 30-Hz, 10-ms pulses were applied every 5 s. For tonic stimulation, continuous 2-Hz, 10-ms pulses were used. These phasic and tonic parameters were chosen to have the same number of pulses for a given duration but with distinct temporal pattern. Both phasic and tonic patterns of stimulation were applied for 2 min with intervals of 20–25 min. Animals used for optogenetic experiments were always connected to the preamplifier and Plexon system to continuously acquire EEG and EMG signals for sleep-wake state classification. TTL signals for controlling laser output were split and input into the Plexon acquisition system through an analog input for accurate time stamping of triggered stimulation. All optogenetic experiments with EEG/EMG monitoring were carried out during the light phase (6 PM–6 AM).

To test whether the wake-promoting effect of DRN^{DA} activation was mediated by direct action of DA, DRN^{DA-ChR2} and DRN^{DA-eGFP} mice that were habituated to the recording setup were systemically administered dopamine receptor antagonists SCH-23390 (a selective D1 antagonist, 1 mg/kg) and eticlopride (a selective D2 antagonist, 1 mg/kg) 45 min before the onset of the light phase. The concentration of these dopamine antagonists was selected based on a previous literature (Eban-Rothschild et al., 2016). For controls, we injected sterile saline at the same circadian time. EEG/EMG recording and phasic optogenetic stimulation started at the light phase onset and lasted for 2 hr.

To study whether the wake-promoting effect of optogenetic DRN^{DA} stimulation is influenced by homeostatic sleep pressure, DRN^{DA-ChR2} or DRN^{DA-eGFP} mice were sleep deprived for 0 or 4 hr by gentle handling (Eban-Rothschild et al., 2016). The order of experiments (0 or 4 hr deprivation) was counter-balanced across animals. For sleep deprivation, mice were continuously monitored by an experimenter (with EEG and EMG recordings turned on). Mice were softly touched by a brush whenever they become motionless and/or exhibited reduced EMG tone or absent EMG bursts. After the sleep deprivation procedure, two phasic bursts (30 Hz, 15 pulses, 10 ms width, 5 s interval) were applied about 5–10 min after they entered into NREM sleep, and the latency to wake transitions was measured.

To study the causal effect of increased DRN^{DA} activity on locomotion, we performed the open field test with DRN^{DA-ChR2} and DRN^{DA-eGFP} mice. Procedures and experimental equipment were similar those described above for open field testing during fiber photometry, with video monitoring and subject position and velocity tracking recorded throughout all sessions. Mice were first habituated in the open field for 20 min. After acquiring 20 min of baseline activity (not including habituation), laser stimulation (phasic or tonic patterns) was delivered for 5 min. After stimulation, five additional minutes were recorded. Throughout testing, distance traveled during 5 min epochs (before, during, and after stimulation) were analyzed.

For chemogenetic experiments, animals with hM4Di-mCherry or eGFP injection were connected to the data acquisition system for EEG and EMG signals. Animals were habituated to experimenter handling for 3–4 days before any experiments commenced. Saline or clozapine-N-oxide (CNO, selective ligand for hM4Di, 1 mg/kg dissolved in saline; Enzo Life Sciences Inc., Exeter, UK) was intra-peritoneally injected immediately prior to the start of testing at 9 AM (3 hr after dark phase onset). Recordings were carried out for 2 hr following injection.

To test whether DRN^{DA} neuronal activity is required for wake maintenance after exposure to salient environmental stimuli, DRN^{DA-hM4Di} or DRN^{DA-eGFP} mice (which were already habituated to experimenter's handling) were first injected with saline or CNO (1 mg/kg) 45 min before testing. Then, a female mouse (contained in an inverted wire cup, thus not directly accessible for mounting) or a filter paper with predator odor TMT was introduced into the recording cage. We chose these two stimuli because they are of opposite valence (positive versus negative) and were shown effective in inducing robust DRN^{DA} neuronal activity (See Figures 1 and S2). EEG/EMG recording began immediately after introduction of the salient stimulus and lasted for 1 hr.

Auditory cue arousal test

To examine whether DRN^{DA} firing mediates cue-induced arousal from sleep, we performed simultaneous recording of fiber photometry and EEG/EMG signals on DRN^{DA-GCaMP6s} mice. On each experimental day, recordings began at the light phase onset (6PM). Auditory tonal stimuli (65 dB; 2, 3, or 5 kHz frequency; 2-Hz pulse; 250-ms pulse width, 10 s duration) were randomly applied during the first half of the light phase (for 6 hr) with a minimum inter-trial interval of 15 min from a speaker located adjacent to the testing cages. In order to limit habituation to specific tonal frequencies, three different tones were administered in random order with a 33.3% probability for each frequency. The speaker was placed 30 cm away from the cage, and the auditory tone intensity inside the cylindrical cage was calibrated with a sound meter (Digital Sound Level Meter, Foneso, Shenzhen, China) before the beginning of each session with mice temporarily removed from the room. TTL pulses time-locked to the auditory cues were generated and inputted into the Plexon data acquisition system for accurate time stamping.

Sleep-wake states were classified as described above by an experimenter (J.R.C.) who was blind to the experimental conditions. Depending on the behavioral consequence of auditory cues, each trial was classified as 1) sleep-to-wake transitions (further divided from NREM or from REM sleep), 2) sleep-to-sleep (when auditory cue failed to induce wakefulness), and 3) wake-to-wake (auditory stimuli that were administered during wakefulness) cases. In order for a trial to be scored as a sleep-to-wake transition, animals had to show at least 3 s of wake EEG and EMG signs (EEG: desynchronized from delta or theta rhythm, EMG: sudden phasic elevation of muscle activity) within 10 s of the auditory cue onset. If these criteria were not met, the trial was categorized as sleep-to-sleep.

To test for the necessity of DRN^{DA} firing in auditory cue-induced arousal from sleep, we inhibited DRN^{DA} neurons in a time-locked manner with the inhibitory proton pump eArch3.0 (Arch). The experimental setup was identical to the procedure described above, except we used a slightly higher intensity tone (70 dB) to avoid possible floor effects, and 20 s of 532 nm green laser (10 mW at the tip) was continuously applied surrounding the tone presentation (starting 5 s before the tone, terminating 5 s after the end of the tone) to the DRN^{DA-Arch} or DRN^{DA-eGFP} mice. Only data epochs when auditory cues were turned on during NREM or REM sleep were considered and we manually reviewed whether auditory tones caused wake transitions (see above for specific criteria). If cues successfully woke up the animal, they were categorized as ‘NREM-to-Wake’ or ‘REM-to-Wake’ trials. If tones did not lead to immediate wake transitions, they were categorized as ‘NREM-to-NREM’ or ‘REM-to-REM’ trials. To confirm that sleep-related oscillations (delta for NREM and theta for REM) were not perturbed in ‘NREM-to-NREM’ and ‘REM-to-REM’ trials, we calculated the delta and theta amplitude for NREM and REM, respectively, and determine whether there were any changes across the tone onset (see Figure S6H-S6K).

Data analysis

Fiber photometry data processing and analysis

Acquired data files were loaded and processed with custom-written codes in MATLAB. Pre-processing was performed as previously described (Lerner et al., 2015). Fiber photometry traces from 490 and 405 nm excitation wavelengths were first low-pass filtered at 2 Hz using a 4th order Butterworth filter with zero-phase distortion. To calculate ΔF/F, a linear fit was applied to 405-nm signal and aligned to the 490-nm signal. The fitted 405-nm signal was subtracted from the 490-nm signal and then divided by the fitted 405-nm signal again to yield the ΔF/F time-series.

To visualize peri-event photometry traces, ΔF/F data epochs were extracted around immediately before and after relevant behavioral events (e.g., event onsets identified by either video scoring or TTL pulses) and averaged. For statistical comparison between baseline and behavior, areas under the curve (AUC) per second values were calculated for given conditions. Similarly, to visualize Ca²⁺ fluorescence change across state transitions, the temporal location of state transitions were identified, and 120 s of photometry traces around the transition time points were extracted and averaged. AUC was also calculated to compare DRN^{DA} population activity before and after transitions. We performed analyses for NREM-to-wake, REM-to-wake, wake-to-NREM, and NREM-to-REM transitions. We excluded other possible combinations as rodents rarely transit directly from REM to NREM, and none of the tested mice showed wake-to-REM transitions, which is a common feature of narcolepsy. We termed periods of less than 15 s of wakefulness after REM state as “short arousal” and we separately plotted these transitions as “REM-to-short arousal-to-NREM” (See Figure S3L).

To detect Ca²⁺ peak events from photometry traces and quantify them across sleep-wake states, we first normalized the trace using z-score and then high-pass filtered at 0.01 Hz using 2nd order butterworth filter with zero-phase distortion to eliminate possible low-frequency fluctuations across states. Then we detected prominent Ca²⁺ peak events with an amplitude threshold, which was defined as the 75th percentile of the entire photometry data amplitude distribution. This percentile threshold was heuristically chosen because the photometry amplitude distribution is positively skewed and does not follow Gaussian distribution, which makes it more sensitive to the presence of outliers (such as during Ca²⁺ peak events). For quantification of these detected events, we calculated 1) peak amplitude, 2) duration (from detection onset to offset), 3) frequency or number of events in a 5 s window, and 4) summed AUC values of detected events in a 5 s window.

In order to account for inter-subject variability in amplitude during investigations into the temporal dynamics of DRN^{DA} activity during each behavioral state from onset to offset, we first converted the fluorescence traces into z-scores (calculated from the entire traces). Next, photometry traces from each state including 10% of the trace before and after were cropped and down-sampled to 120 points in order to normalize the timescale. This allowed us to project variable length photometry traces containing z-score normalized fluorescence changes onto the normalized time of –0.1 to 1.1, where 0 notes the onset and 1 notes the offset of a wake or sleep episode.

To examine any correlation between DRN^{DA} activity and locomotion, we obtained the synchronized recordings of fiber photometry and video tracking. To test if increased DRN^{DA} activity is associated with any change in locomotion, we detected prominent Ca²⁺ peak events as previously described above, extracted 10 s of velocity traces around peak event onsets, and then averaged. Conversely, to test if initiation of locomotion is associated increased DRN^{DA} activity, we detected locomotion onset similarly as the Ca²⁺ peak events (but with 65th percentile as an amplitude threshold), extracted 10 s of photometry traces around locomotion onsets, and then averaged.

EEG spectrogram

To visualize spectral and temporal profiles of EEG activity across distinct behavioral states, we decomposed EEG into time-frequency plan using Morlet wavelet. EEG data epoch of interest was convolved with a complex Morlet wavelet, $w(t, f_0)$, having a Gaussian shape both in the time (σ_t) and frequency (σ_f) domain around its central frequency, f_0 :

$$w(t, f_0) = \left(\frac{\sigma_f}{\pi}\right)^{-1/2} \exp\left(-\frac{t^2}{2\sigma_t^2}\right) \exp(2i\pi f_0 t), \text{ where } \sigma_f = 1/2\pi\sigma_t.$$

A wavelet family was characterized by a constant (f_0/σ_f) ratio of 6 from 1 to 20 Hz in 1 Hz steps. The time-varying energy of the signal, $E(t, f_0)$, is defined as the squared norm of the convolution product of a complex wavelet $w(t, f_0)$, with the signal $s(t)$: $E(t, f_0) = |w(t, f_0) \times s(t)|^2$.

Time-varying energy is then smoothed by a moving average filter with span of 2 s for each frequency step to enhance visualization.

Calculation of EEG frequency band

To extract time-varying amplitude of a certain EEG frequency band (e.g., 0.5–4 Hz for delta, 5–10 Hz for theta, and 40–100 Hz for high-frequency – notch filter was applied from 58 to 62 Hz before calculating high-frequency activity amplitude to avoid any contribution from 60 Hz line noise), the signal of interest was first band-pass filtered using a 2nd order Butterworth filter. A zero-phase shift filter was used to prevent any phase distortion. Instantaneous amplitude was obtained by taking the absolute value of the Hilbert transform of the band-passed signal. EEG frequency band amplitude signals were smoothed by a moving average filter (with 10 s window for Figures 4 and S4 and with 2 s window for Figures 6 and S6) and then normalized using z-score with respect to the baseline. EEG data epochs containing high-amplitude artifacts were excluded from analysis.

Power spectral density

Power spectral density was estimated for EEG data using a Welch's method. We used a 5 s window size and 50% overlap to estimate power from 0.5 to 100 Hz (except from 58 to 62 Hz). For 1 hr chronic optogenetic stimulation, spectral power changes during optogenetic stimulation with respect to the baseline (1 hr before the stimulation) were obtained for both DRN^{DA-ChR2} and DRN^{DA-eGFP} mice. For chemogenetic experiments, spectral power changes of CNO conditions from saline conditions were calculated at each frequency step. EEG data epochs with high-amplitude artifacts were excluded from analysis.

Efficiency and specificity of GCaMP6f+ expression

Efficiency was defined as “the number of GCaMP6f+ and TH+ neurons out of the total number of TH+ neurons.” Specificity was defined as “the number of GCaMP6f+ and TH+ neurons out of the total number of GCaMP6f+ neurons.”

Ex vivo electrophysiology

TH-cre mice expressing ChR2-eYFP or hM4Di-mCherry were euthanized with carbon dioxide and transcardially perfused with ice-cold sucrose-based cutting solution saturated with 95% O₂/5% CO₂ (carbogen) that contained (mM) 85 NaCl, 75 sucrose, 2.5 KCl, 1.25 NaH₂PO₄, 4.0 MgCl₂, 0.5 CaCl₂, 24 NaHCO₃ and 25 glucose. The brain was removed and 250-μm coronal slices that contained the DRN were prepared in oxygenated cutting solution using a vibratome (VT-1200, Leica Biosystems, IL, USA). Slices were recovered at 32°C for one hour prior to recording in carbogenated ACSF containing (mM): 125 NaCl, 2.5 KCl, 1.2 NaH₂PO₄, 1.2 MgCl₂, 2.4 CaCl₂, 26 NaHCO₃, and 11 glucose. Slices were transferred to the recording chamber and perfused (1.5 - 2.0 mL/min) with carbogen-saturated ACSF at 32 ± 0.5°C. Whole-cell patch clamp recordings of fluorescently tagged (TH+) DRN neurons were obtained using a MultiClamp 700B amplifier (Molecular Devices, CA, USA) and a Digidata 1440 analog-to-digital converter (Molecular Devices). Data were sampled at 10 kHz and filtered at 2 kHz with Clampex 10.4 (Molecular Devices). Patch electrodes had resistance of 4 - 6 MΩ and were filled with a potassium gluconate intrapipette solution (mM): 135 K gluconate, 5 KCl, 5 EGTA, 0.5 CaCl₂, 10 HEPES, 2 Mg-ATP, and 0.1 GTP. Electrophysiological data were analyzed with Clampfit 10.4 (Molecular Devices). For Figure S4A, light-evoked currents (voltage clamp) and action potentials (current clamp) were evoked by ten of 30 Hz (10 ms pulse width) blue (420–455 nm) light delivered by an LED light source (Lumencor, OR, USA) in neurons held at -70mV. Once we patched hM4Di-mCherry+ or eGFP+ DRN^{DA} cells (Figures S5A–S5E), neuronal firing was evoked by depolarizing the membrane potential to -45 mV in current clamp mode. After collecting baseline for ~2 min, 1 μM of CNO was applied to the bath for neuronal silencing. After 3-4 min, CNO was washed out.

Histology

Perfusion

Mice were euthanized with CO₂ and transcardially perfused with 20 mL of ice-cold 1x PBS with heparin (10 U/mL) and then with 30 mL of ice-cold 4% PFA in 1x PBS. Mouse brains were carefully removed from the skull and post-fixed in 4% PFA at 4°C overnight. The 4% PFA solution was switched to 1x PBS in the morning. Brains were sectioned into 50 μm coronal slices with a vibratome (VT1200, Leica Biosystems, IL, USA). Slices were stored in 1x PBS at 4°C until immunohistochemical processing.

Immunohistochemistry

Brain sections were incubated in a 1x PBS solution containing 0.1% Triton X-100 and 10% normal donkey serum (NDS; Jackson ImmunoResearch, PA, USA) with primary antibodies (see below for details) at 4°C overnight. Afterward, sections were thoroughly washed four times (15 min each) in 1x PBS and temporarily stored at 4°C. Sections were then transferred into a secondary antibody cocktail, which included 1xPBS with 0.1% Triton X-100, 10% NDS with secondary antibodies (see below for details), and stored at 4°C overnight. The next morning, sections were again washed by 1x PBS solution four times (15 min each), mounted on glass microscope slides (Adhesion Superfrost Plus Glass Slides, #5075-Plus, Brain Research Laboratories, MA, USA), dried, and cover-slipped with a DAPI-containing mounting media (Fluoromount G with DAPI, 00-4959-52, eBioscience, CA, USA).

Antibodies

For primary antibodies, anti-chicken TH (1:500; TYH, Aves Labs, OR, USA), anti-rabbit TH (1:500; sc-14007, Santa Cruz Biotechnology, CA, USA), anti-chicken GFP (1:500; GFP-1020, Aves Labs), anti-goat 5HT (1:1000; 20079, ImmunoStar, WI, USA), and anti-rabbit mCherry (1:500; ab167453, Abcam, Cambridge, UK) were used. For secondary antibodies, anti-chicken/rabbit Alexa

Fluor 488 (1:500; 703-545-155, 711-545-152, Jackson ImmunoResearch), anti-goat/rabbit Rhodamine Red-X (1:500; 705-297-003, 711-297-003, Jackson ImmunoResearch), and anti-rabbit/chicken Alexa Fluor 647 (1:500, 711-607-003, 703-606-155, Jackson ImmunoResearch) were used.

Confocal microscopy imaging

Fluorescent images from brain tissue were acquired by a LSM 780 confocal microscope (Carl Zeiss, Jena, Germany). We used a 10x Plan Apochromat air objective (NA 0.45), 25x Plan Apochromat water immersion objective (NA 1.2) and 4 laser wavelengths (405 nm, 488 nm, 561 nm, and 633 nm). Image acquisition was controlled by Zen 2011 software (Zeiss), which also allowed automated z stacking, tiling, and maximum intensity projection. Images were not further processed.

QUANTIFICATION AND STATISTICAL ANALYSIS

All data are represented as mean \pm SEM. Sample sizes were determined to be comparable to previous studies that used optogenetics or chemogenetics to study neural circuits of sleep and wake state regulation ([Xu et al., 2015](#); [Eban-Rothschild et al., 2016](#)). All statistical analyses were performed with in-built functions of the Statistics and Machine Learning toolbox in MATLAB (Mathworks) or Prism (GraphPad). Paired and unpaired t tests were used for single value comparisons. One-way ANOVA was used to compare more than two groups. Two-way repeated-measures ANOVA was used to perform group comparisons with multiple measurements. Data are considered to be statistically significant if $p < 0.05$. We used Bonferroni correction to control for multiple comparisons where appropriate.